CATALYTIC REACTION OF MEDIATED OXIDATION IN ETHYLBENZENES AND BENZYL ALCOHOL USING GOLD SUPPORTED ON ZINC OXIDE CATALYST

AFIQ BIN ANWAR

FACULTY OF SCIENCE
UNIVERSITI MALAYA
KUALA LUMPUR

2022

CATALYTIC REACTION OF MEDIATED OXIDATION IN ETHYLBENZENES AND BENZYL ALCOHOL USING GOLD SUPPORTED ON ZINC OXIDE CATALYST

AFIQ BIN ANWAR

DISSERTATION SUBMITTED IN FULFILMENT OF THE REQUIREMENTS FOR THE DEGREE OF MASTER OF SCIENCE

DEPARTMENT OF CHEMISTRY
FACULTY OF SCIENCE
UNIVERSITI MALAYA
KUALA LUMPUR

2022

UNIVERSITI MALAYA

ORIGINAL LITERARY WORK DECLARATION

Name of Candidate: **AFIQ BIN ANWAR**

Registration/Matric No: **17005720/1 (SGR150011)**

Name of Degree: **MASTER OF SCIENCE**

Title of Project Thesis ("this Work"):

CATALYTIC REACTION OF MEDIATED OXIDATION IN ETHYLBENZENES AND BENZYL ALCOHOL USING GOLD SUPPORTED ON ZINC OXIDE CATALYST

Field of Study: **CATALYSIS**

I do solemnly and sincerely declare that:

(1) I am the sole author/writer of this Work;
(2) This Work is original;
(3) Any use of any work in which copyright exists was done by way of fair dealing and for permitted purposes and any excerpt or extract from, or reference to or reproduction of any copyright work has been disclosed expressly and sufficiently and the title of the Work and its authorship have been acknowledged in this Work;
(4) I do not have any actual knowledge nor do I ought reasonably to know that the making of this work constitutes an infringement of any copyright work;
(5) I hereby assign all and every rights in the copyright to this Work to the University of Malaya ("UM"), who henceforth shall be owner of the copyright in this Work and that any reproduction or use in any form or by any means whatsoever is prohibited without the written consent of UM having been first had and obtained;
(6) I am fully aware that if in the course of making this Work I have infringed any copyright whether intentionally or otherwise, I may be subject to legal action or any other action as may be determined by UM.

Candidate's Signature Date: 9.1.2022

Subscribed and solemnly declared before,

Witness's Signature Date: 9.1.2022

Name:

CATALYTIC REACTION OF MEDIATED OXIDATION IN ETHYLBENZENES AND BENZYL ALCOHOL USING GOLD SUPPORTED ON ZINC OXIDE CATALYST

ABSTRACT

Gold nanoparticles of 3 nm supported on zinc oxide was synthesized by urea deposition precipitation then utilized as a catalyst in ethylbenzene and benzylalcohol oxidation using tert-butyl hydroperoxide as the oxidant in acetonitrile solvent. The catalyst gave more than 50% conversion and high selectivity towards acetophenone (50%) as the major product but moderate selectivity towards other products such as 1-phenylethanol, benzaldehyde, benzoic acid, and other compounds in 5 mL acetonitrile solvent at 100 °C for 24 hours reaction. The catalyst showed high selective for benzylalcohol oxidation with 60.3 % conversion and 100 % selectivity towards benzaldehyde. The fresh and spent catalysts were comprehensively characterized by XRD, HRTEM, XRF, BET and ATR-IR to correlate the catalyst activity. Factors affecting the catalytic activity in ethylbenzene oxidation such as gold loading, calcination treatment at 300 °C, type of solvent, reaction time, reaction temperature, oxidant to ethylbenzene molar ratio, catalyst weight and solvent volume were studied. The gold nanoparticle introduces a very selective reaction pathway and is an environmentally friendly catalyst as the oxidant used is less harmful.

Keywords: gold nanoparticles, zinc oxide support, deposition precipitation, ethylbenzene oxidation, benzyl alcohol oxidation.

REAKSI KATALITIK PENGOKSIDAAN PERANTARA DALAM ETILBENZENA DAN BENZIL ALKOHOL MENGGUNAKAN PEMANGKIN EMAS YANG DISOKONG PADA ZINK OKSIDA

ABSTRAK

Nanopartikel emas berdiameter 3 nm disokong pada zink oksida yang disintesis melalui kaedah pemendapan urea telah digunakan sebagai pemangkin dalam pengoksidaan etilbenzena dan benzil alkohol. Kaedah ini menggunakan tert-butil hidroperoksida sebagai agen pengoksidaan dalam pelarut asetonitril. Pemangkin tersebut memberikan lebih daripada 50% penukaran dan kepemilihan yang tinggi terhadap asetofenon (50%) sebagai produk utama dengan kepemilihan sederhana terhadap produk lain seperti 1-feniletanol, benzaldehid, asid benzoik dan kompoun lain dalam pelarut 5 ml pelarut asetonitril pada suhu 100 ° C selama 24 jam. Pemangkin memberi kepemilihan tinggi untuk pengoksidaan benzil alkohol dengan penukaran 60.3% dan 100% kepemilihan terhadap benzaldehid. Pemangkin baru dan telah digunakan juga melalui beberapa ujian pencirian, seperti XRD, HRTEM, XRF, BET dan ATR-IR. Faktor yang mempengaruhi aktiviti pemangkinan di dalam pengoksidaan etilbenzena seperti pemuatan emas, kaedah pembakaran pada 300 ° C, jenis pelarut, masa tindak balas, suhu tindak balas, nisbah molar oksida, berat pemangkin dan isipadu pelarut dikaji. Nanopartikel emas memperkenalkan laluan tindak balas yang sangat selektif (memilih) dan merupakan pemangkin mesra alam kerana pengoksida yang digunakan kurang memberi mudarat pada alam sekitar.

Kata kunci: nanopartikel emas, penyokong zink oksida, kaedah pemendapan, pengoksidaan etilbenzena, pengoksidaan benzil alkohol.

ACKNOWLEDGEMENTS

First and foremost, Alhamdulillah for the time and patience that Allah granted me in completing this project. I would also wish to convey my sincerest gratitude to many parties that my heartfelt thanks go to my supervisor, Dr. Azman Ma'amor and co-supervisor Associate Professor Dr. H.N.M. Ekramul Mahmud who provides me with insightful comments and guidance throughout this project. Furthermore, a huge gratitude to them for their time and willingness in helping me editing the contents of the thesis.

In order to be able to complete this project successfully, I would like to thank the laboratory staff at Department of Chemistry, Department of Physics and INFRA Lab of University Malaya in helping me in the testing and analysis of my project. I also would like to acknowledge my colleagues at Department of Chemistry whom willing to share their ideas, information and allow me to have a good discussion.

This research was supported by a by the University Malaya Research Grant (RP005C-13AET) and Postgraduate Research Grant (PG201-2016A) for the sources of funding throughout this study. I gratefully acknowledge UM for financial support (Graduate Research Assistantship Scheme) and MyMaster scholarship from Kementerian Pendidikan Malaysia (KPM) that helping me in this study.

Last but not least, my huge thanks go to my family, especially my mother Faizah Ahmad that unconditionally helping me in the progress of my thesis. Mama thank you for being there for me at all times, supporting me and keep pushing me in completing my project.

Sincerely,

Afiq Anwar

TABLE OF CONTENTS

LIST OF FIGURES

LIST OF TABLES

LIST OF SYMBOLS & ABBREVIATION

ACP	:	Acetophenone
ACN	:	Acetonitrile
ATR-FTIR	:	Attenuated Total Reflectance - Fourier Transform Infrared
AuNPs	:	Gold nanoparticles
BA	:	Benzyl alcohol
BET	:	*Brunauer-Emmett-Teller*
BzA	:	Benzoic Acid
BZL	:	Benzaldehyde
CP	:	Co-precipitation
DP	:	Deposition Precipitation
DPU	:	Deposition Preciptation with Urea
EB	:	Ethylbenzene
GC-FID	:	Gas Chromatography – Flame Ionization Detector
HRTEM	:	High Resolution Transmission Electron Microscopy
MB	:	Methylbenzoate
PE	:	1-phenylethanol
t-BHP	:	tert-Butyl Hydroperoxide
THF	:	Tetrahydrofuran
Wt %	:	Weight percent loading
XRD	:	Xray Diffraction
XRF	:	Xray Fluorescence

LIST OF APPENDICES

CHAPTER 1: INTRODUCTION

1.1 Research Background

Nanotechnology is science, engineering, and technology conducted at the nanoscale, which is about 1 to 100 nanometers. The birth of nanoscience started with a physicist Richard Feynman, also known as the father of nanotechnology. In "There's Plenty of Room at the Bottom" lecture on December 29, 1959, Feynman described scientists would be able to manipulate and control individual atoms and molecules. A decade later, Professor Norio Taniguchi coined the term nanotechnology. Nanomaterial have widely used in drug delivery, chemical sensors, biosensors, fuel cells, and catalysis. There are several types of nanomaterial such as metal nanoparticles, semiconductor nanocrystals, organic polymers, graphene and carbon nanotubes (Hulla et al., 2015). Materials in nanometre size show distinct properties from their bulk counterparts because nano-sized clusters have an electronic structure with high dense states (Dehghan Banadaki & Kajbafvala, 2014). One of the emerging nanomaterials that has been used as heterogenous catalysis is Gold. Gold is a transition metal with the least reactive chemical elements (noble metals) due to its stable and balanced electron configurations. The bright yellow dense, soft, malleable and ductile metal which is gold naturally occur in the form of nuggets or grains. Due to lower melting point of gold (1063 °C) when compared to platinum (1772 °C) gold is regarded as precious metal that commonly used in jewellery and decorations crafting. However, gold used to be considered as poor catalytic species when compared to palladium, platinum or ruthenium due its bulk sized. When gold is downsized to nanoscale, it has unique optical, electronic and catalytic properties (Roduner, 2006).

The first colloidal gold nanoparticles at 30 nm size was successfully prepared by the reduction of gold chloride with phosphorus in water by Michael Faraday 160 years ago which leads for the application of wine color stained on the glass window of cathedrals and churches (Haruta, 2011). Further findings proves the size of gold particles provide a unique optical properties at particle size below 50 nm as it gives wine red color (Edwards & Thomas, 2007) whereas at 400 nm AuNPs shows light purple (Priecel et al., 2016). As the particle size increases, the surface plasmon resonance wavelength shifts IR spectrum and giving a clear or translucent colour (Chandra et al., 2013). Among the heterogeneous metal catalyst, gold was considered catalytically inactive since 1960 despite the studies of Zsigmondy in 1909 which used the reducing agents to control the size of gold colloids (Bond, 2008; Haruta, 2011). However in 1973, Bond reported the hydrogenation of olefins over supported gold catalysts prepared via impregnation of HAuCl4 (Bond et al., 1973). Even then, gold was not recognized as an efficient catalyst since it was ineffective and not a viable alternative compared to well dispersed palladium or platinum. The catalytic activity of gold was later discovered by Haruta and Hutching research groups (Bond et al., 2006), in the oxidation of CO at low temperature (Haruta et al., 1987) and the hydro-chlorination of acetylene to vinyl chloride, respectively (Hutchings, 1985). Both groups reported that the catalytic activity of gold particles could be enhanced when presence in nanoscale dimensions (Fang et al., 2017; Haruta, 2004; Haruta, 2014; Masatake, 2003; Torres et al., 2016). On top of that, gold is the most efficient nanoparticle catalyst for a different type of aerobic (low-cost) oxidation reaction as it has shown promising behavior in selectivity and resistance to catalyst deactivation compared to Pd and Pt catalysts (Mallat & Baiker, 2004).

In classical chemistry, gold was used in a form of thin wires for electrical connections because of its chemical inertness and high electrical conductivity. Nowadays, nanoscale gold catalyst is widely regarded as the best green catalytic

material for various processes and applications such as the selective oxidation of alcohols (Philip et al., 2017), hydrogenation of nitro compounds (Torres et al., 2016), laser ignition (Fang et al., 2017), cosmetic (Jiménez-Pérez et al., 2017), photocatalysis (Khan et al., 2017; Tan et al., 2017), sensor for visual detection of pork adulteration (Ali et al., 2012), as therapeutic agent (Raliya et al., 2017), photodynamic therapy (Lucky et al., 2015), act as probes in dark field microscopy (Ma et al., 2016), act as bio-marker for heart disease diagnosis (Wong et al., 2014), glycosylation of carbohydrate (Pflästerer & Hashmi, 2016), pollution and emission control applications (Engel & Ertl, 1979; McClure & Goodman, 2009), clean hydrogen production for fuel cells (Bond et al., 2006) , sensors to detect poisonous, flammable substances in solution (Fackler, 2007), for air cleaning at room temperature and green production for chemicals (Takei et al., 2012).

1.2 Problem Statement

Alkyl benzene and aromatic alcohol oxidation proves to be the most important reactions in the manufacturing of soap and perfumes (Xia et al., 2012). At present, industrial practice applies high temperature thermal autoxidation in the absence of heterogeneous catalyst. The oxidation requires the usage of potassium permanganate and potassium dichromate that typically produces toxic, non-environmentally friendly and hazardous waste (Sheldon et al., 2007). Current findings show that the supported metal catalyst can be used in this particular reaction (Ali et al., 2014). Supported platinum group catalyst can be used in the oxidation of alcohols, yet it often requires a promoter to increase the selectivity and stability for such reactions. Oxidants such as oxygen, hydrogen peroxide, tert-butyl hydroperoxide (TBHP) and iodoxybenzoic acid (IBX) (Dapurkar et al., 2009; Zhu et al., 2007) could successfully convert the alkyl benzene to a desired product. However, it is a challenge to achieve a conversion higher than 90% especially in ethylbenzene oxidation since it is difficult to activate the ethyl

carbon branch in oxidation reaction. Most of the ethylbenzene oxidation using heterogenous catalyst demonstrated conversion less than 90% in solvent system with low acetophenone (ACP) selectivity in reaction atmosphere: air (Biradar & Asefa, 2012; Habibi et al., 2014; Vetrivel & Pandurangan, 2004). Other catalysts for the oxidation of ethylbenzene such as zeolite Beta containing ultra-small CoO particles and MnFeSi composite also demonstrated low conversions, which produce acetophenone as the major product, together with 1-phenylethanol, 1-phenylethyl hydroperoxide, benzoic acid and benzaldehyde as the by-products (Oliveira et al., 2017; Zhang et al., 2017). It is well known that gold supported metal oxides are very active oxidants for CO oxidation (Qiao et al., 2016), but the oxidation of ethylbenzene and benzyl alcohol using AuNPs supported on ZnO is yet to be reported.

The main motivation and focus of this research is to develop an environmental friendly and more efficient catalytic system using non-toxic gold supported catalysts for the oxidation of alkyl benzene and benzyl alcohol in order to replace the existing usage of potassium permanganate and potassium dichromate catalyst for such reactions.

1.3 Scope of Present Work

The gold nanoparticle synthesized via deposition precipitation method was found to be promising compared with other methods in the oxidation of ethylbenzene and benzylalcohol. The catalyst was characterized using HR-TEM, XRD, ATR-IR, BET and XRF analysis. Several studies on the effect of certain parameters, such as the weight of catalyst, volume of reactant, molar ratio of oxidant, reaction temperature, reaction time, amount of gold wt%, effect of calcination, and type of solvents were varied and tested using synthesized AuNPs on ZnO catalyst. In addition, the catalyst stability and recyclability also were studied.

1.4 Objectives

The objectives of this study are listed as follows:

1. To synthesize the supported nanoparticle gold catalysts on zinc oxide via deposition precipitation method.
2. To characterize the supported nanoparticle gold catalysts on zinc oxide via several analytical methods, namely, HR-TEM, XRD, ATR-IR, BET and XRF.
3. To evaluate the catalytic performance of the synthesized catalyst in ethyl benzene and benzyl alcohol oxidation reaction.

1.5 Organization of Thesis

This thesis has been structured into 5 respective chapters.

Chapter 1 - Present a general review of the project including the problem statement, research overview and objectives of the study.

Chapter 2 - Highlight on the literature review and research background of the gold catalyst synthesis methods and catalysis of ethylbenzene and benzylalcohol.

Chapter 3 - Describe on the synthesizing of gold nanoparticles on zinc oxide (Au/ZnO) using deposition precipitation method and its characterization followed by analysis of the oxidation products.

Chapter 4 - Discussion on the characterization of synthesized AuNPs on ZnO, Catalytic studies of ethylbenzene and benzyl alcohol using AuNPs on ZnO and catalyst stability.

Chapter 5 - Conclude on the overall results and recommendation for future research proposal of this study.

CHAPTER 2: LITERATURE REVIEW

2.1 Catalysis

Catalysis was first started when the people began to use catalysts in the production of wine and beer by fermentation ("Chapter 1 History of catalysis," 1993; Lindström & Pettersson, 2003). Nowadays, catalysis has rapidly growth and gives a significant impact in chemical industry such as petrochemicals, pharmaceuticals, petroleum and pollution control (Viswanathan et al., 2002). The term catalysis was first used in 1836 by Berzelius which in the study of the effect of porous platinum on the combustion of hydrogen and oxygen at ambient temperatures (Campbell, 1988). Catalyst only functioned to accelerates the reaction at which a chemical system approaches equilibrium, without being consumed in the process by providing a different route which has lower activation energy (Ea) (R.E. Hayes, 2012)

Chemical industries nowadays are strived to achieve the best approach to reduce pollution by developing a new catalytic oxidation to produce desired product with economic feasible and green environment concepts. Catalyst plays a major role in chemical industry from the beginning of 20th century (Kieboom, 1999). In 1990s, the developments of catalyst were started to flourish in US chemical industries as it was reported over 130 examples of new innovative catalyst were used in operating processes. This phenomenon demonstrates the important role of catalytic technology in giving more profitable and high production volume (Armor, 2001).

A good catalyst as proposed by Sabatier must be able to form a relatively stable intermediate adsorption neither too weak nor too strong (Liu, 2011). Characteristics of a good catalyst includes selectively catalyzes the target compound, highly distributed

active phase on the support, a good mechanical strength, capable to withstand high temperature, high surface area and unique porous structure (Furusaki, 2001). There are two important classes of catalysts: homogenous catalysts consisting of aqueous ions that are uniformly mixed with the reactants whereas heterogeneous catalysts provide a surface that holds and reconfigures the reactants in a way that is favorable for reaction. The heterogeneous catalysts usually preferable for the oxidation reaction since most homogenous catalyst such as potassium permanganate, potassium dichromate or ammonium cerium nitrate are too corrosive and required harsh process condition to perform the reaction (Adnan et al., 2015; Biradar & Asefa, 2012). On top of that, homogeneous catalyst appeared to be poor recycling, stability, and handling in industries (Sharma et al., 2016). While, heterogeneous catalysis involving solid catalyst is more attractive as they facilitate high turnover and it can be recovered and reused (Titinchi et al., 2015).

Catalysts are widely used especially in industrial production such as in automobile exhaust, Haber-Bosch process (ammonia production), contact process (sulphuric acid production) and others. Catalyst always related with high acceleration rate and produce product cheaper with high purity. Currently, Haber-Bosch process uses potassium promoted iron-based catalyst because potassium is helping iron in dissociative adsorption of N_2 process on catalyst surface. Temprano and Jenkins used iron pyrite in their production of ammonia at low temperatures under ultra-high vacuum condition (Rafiqul et al., 2005).

Catalytic AuNPs have great prospects in environmentaly friendly and green sustainable chemical processes because of the high activity at room temperature and possess high oxygen storage capacity which is suitable for oxidation reaction (Mallat & Baiker, 2004).

2.1.1 Ethylbenzene Oxidation

Ethylbenzene is a highly flammable, colourless liquid with an odour like gasoline, commonly found in natural products such as coal tar and petroleum and in manufactured products such as inks, insecticides and paints. The heterogeneous catalytic oxidation of ethylbenzene is a very attractive process from an economic and environmental point of view as its yields acetophenone and 1-phenylethanol. Figure 2.1 shows proposed a mechanism by Biradar and Asefa on nanoporous silica-supported gold nanoparticle catalyst and its selective oxidation of alkyl substituted that the catalytic reaction can only work at high temperatures (120–150 ºC) (Biradar & Asefa, 2012).

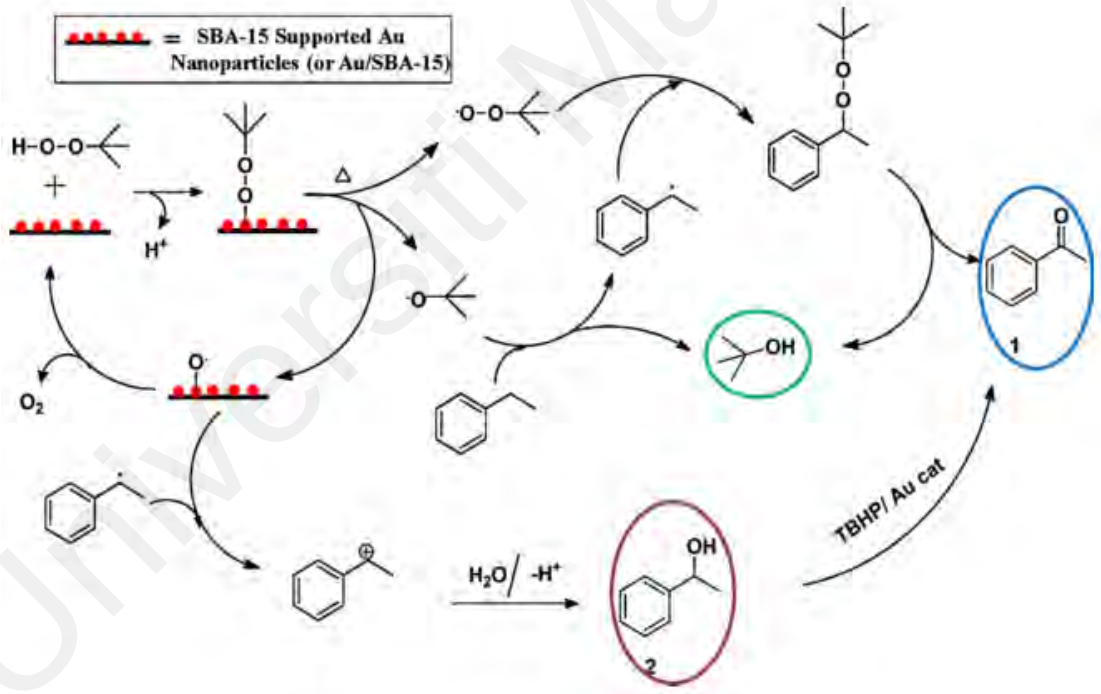

Figure 2.1: Proposed mechanism of ethylbenzene oxidation (Biradar & Asefa, 2012) (Reproduced with permission).

Figure 2.2 shows a oxidation reaction of ethylbenzene which produces acetophenone as major product and widely used in fragrance and resin while 1-phenylethanol is mostly used as precursor for the preparation of analgesic and anti-inflammatory drugs (Ali et al., 2014; Chaudhary & Sharma, 2020; Ji et al., 2021).

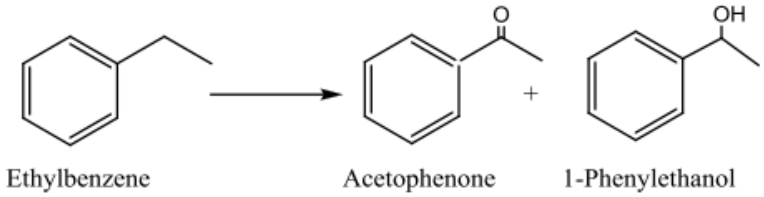

Figure 2.2: Oxidation of ethylbenzene (Ali et al., 2014) (Reproduced with permission).

Oxidant is essential to supply oxygen molecules in ethylbenzene oxidation reaction. Usually, homogeneous oxidants like CrO_3, $KMnO_4$, MnO_2 and SeO_2 are also employed. For the demand of green chemistry concept these oxidants should be replaced with cleaner oxidant like molecular oxygen or aqueous hydrogen peroxide (Zhan & Thompson, 2004). However, these oxidants require highly active, selective and recyclable O_2-activating heterogeneous catalyst (Wang et al., 2006).

Several metal complexes were used in ethyl benzene oxidation. Lu and co-worker using 8-quinolinolato manganese (III) complexes as catalyst for the oxidation of ethylbenzene with hydrogen peroxide (H_2O_2) demonstrated 26% conversion and 65% yield of acetophenone (Lu et al., 2010). Kanjina and Trakarnpruk later studied the solvent free oxidation of ethylbenzene to acetophenone using t-BHP as an oxidant at 130 ℃ for a greener approach. It showed an excellent catalytic performance with mixed metal (MgCuAl) oxide catalyst produced 87 % ethylbenzene conversion and 92 % selectivity towards acetophenone which the catalytic test were carried out in a magnetically stirred stainless steel reactor. However, another by-product (benzaldehyde and benzoic acid) were reported from this reaction alongside 1-phenylethanol. With regards to reusability, it was found that the mixed metal oxide catalyst demonstrated a slight drop in activity after the third run due to the decrease in active base sites from their coverage by polar products on the catalyst surface (Kanjina & Trakarnpruk, 2011). Highly efficient solvent-free oxidation of ethylbenzene using t-BHP as oxygen source

over manganese nanocatalysts was reported with 60% conversion and 93% selectivity to acetophenone (Arshadi et al., 2012). Another study of solvent free oxidation of ethylbenzene using Ce-BTC catalyst under 5.5 mL/min air flow rate has been done by Peng and co-workers (M. M. Peng et al., 2014). The expected major product of ethylbenzene oxidation was acetophenone, with a small amount of benzaldehyde and benzoic acid. The Ce-BTC catalyst showed 85 % conversion and 96 % selectivity for 20 hr of reaction time at 160 ℃ and the catalyst is reproducible up to 4 consecutive runs. However, the conversion and selectivity achieved were less than those reported by Devika which used Ce-AlPO-5 catalyst, showed more than 90 % conversion and selectivity to acetophenone consequently at all temperatures which using fixed bed vertical downward flow glass reactor (Devika et al., 2011). Peng and co-workers claimed that the lower conversion observed was likely due to the oxygen involved in the reaction was from air at ambient condition, over the liquid phase. The conversion could increase if the reaction was carried out by bubbling oxygen into the liquid as Ce^{3+} sites on the catalyst would act more efficiently in the conversion.

Habibi designed the selective oxidation of ethylbenzene using Fe/SiO_2-Al_2O_3 nano-catalyst in organic solvent (ACN, dichloromethane, ethanol) with t-BHP as an oxidant showed the highest conversion (35 %) when dichloromethane was used as the solvent, followed by ACN and ethanol. However, ACN showed better selectivity (74 %) towards acetophenone as compared to dichloromethane which only gave only ~68 % selectivity to acetophenone. From the studies, it was found that the optimum condition to get the excellent catalytic performance was done using 50 mg catalyst in 24 h reaction at 100 ℃ (Habibi et al., 2013). Table 2.1 shows a detailed list of the reaction conditions in several studies on oxidation of ethylbenzene.

Table 2.1: Oxidation of ethylbenzene.

Catalyst	Solvent	Time (hr) & Temp (^{o}C)	EB:Oxidant (mole)	Conversion (%)	Selectivity (%)	Reference
MgCuAl	None	18 hrs at 130 ˚C	TBHP (1:3)	90	89 ACP 2 PE 3 BZL 6 BzA	(Kanjina & Trakarnpruk, 2011)
Au/SBA-15	ACN	36 hrs at 70 ˚C	TBHP (1:2)	89	94 ACP 6 PE	(Biradar & Asefa, 2012)
Q_3Mn^{III} complexes	Acetone-water	6 hrs at 30 ˚C	H_2O_2 (2.5:1)	26	70 ACP 30 PE	(Lu et al., 2010)
Ce-BTC	None	20 hrs at 160 ˚C	O_2 (5.5 ml/min)	85	95 ACP 4 BZL 1 BzA	(M. Peng et al., 2014)
CeAlPO-5	CO_2	6 hrs at 175 ˚C	Air (17ml/min)	95	92 ACP 8 Other	(Devika et al., 2011)

Table 2.1, continued.

Catalyst	Solvent	Time (hr) & Temp (^{o}C)	EB:Oxidant (mole)	Conversion (%)	Selectivity (%)	Reference
Fe-SiO_2/Al_2O_3	None	24 hrs at 50 ˚C	TBHP (1:1)	41	89 ACP 11 Other	(Habibi et al., 2013)
2CoSBA-15	ACN	6 hrs at 70 ˚C	TBHP 1:15	12	23 ACP 77 BzA	(Unnarkat et al., 2021)
2CoKIT-6	ACN	6 hrs at 70 ˚C	TBHP 1:15	37	12 ACP 88 BzA	(Unnarkat et al., 2021)
CuMgAl-LDH	Benzonitrile	5 hrs at 100 ˚C (presence of NHPI)	O_2	99	98 ACP 2 Others	(Dai et al., 2021)
Co2Ni1Al1Ox	Acetic acid	10 hrs at 120 ℃	TBHP 1:3	80	89 ACP 9 BZL 2 PE	(Ji et al., 2021)

Table 2.1, continued.

Catalyst	Solvent	Time (hr) & Temp (^{o}C)	EB:Oxidant (mole)	Conversion (%)	Selectivity (%)	Reference
Cu-Co/SAPSi	None	6 hrs at 100 °C	TBHP 1:4	84	87 ACP 13 BZL	(Chaudhary & Sharma, 2020)
Mesoporous CeO_2 nanosphere Ni doped	None	7 hrs at 140 °C	O_2	35	72 ACP 28 PE	(Liu & Zhang, 2020)
NHPI/Co(II)	hexafluoropropan-2-ol (HFIP)	4 hrs at Room Temperature	O_2	88	61 ACP 35 PE 3 BA 1 Other	(Xu et al., 2020)
Zn-Cr-LDH/CNTs	None	6 hrs at 130 °C	O_2	54	94 ACP 2 BZL 4 PE	(Zhao et al., 2018)
Co-N-C-500/SiO_2	None	5 hrs at 120 °C	O_2	30	74 ACP 23 PE 3 BZL	(Liu et al., 2014)

2.1.2 Benzyl Alcohol Oxidation

Benzyl alcohol oxidation has been largely used as a model reaction in aromatic activated alcohols. It is known that several side- products such as benzene, benzoic acid, benzyl benzoate, and toluene are typically formed other than the main product, benzaldehyde. The compounds are shown in Figure 2.3 (Villa et al., 2015).

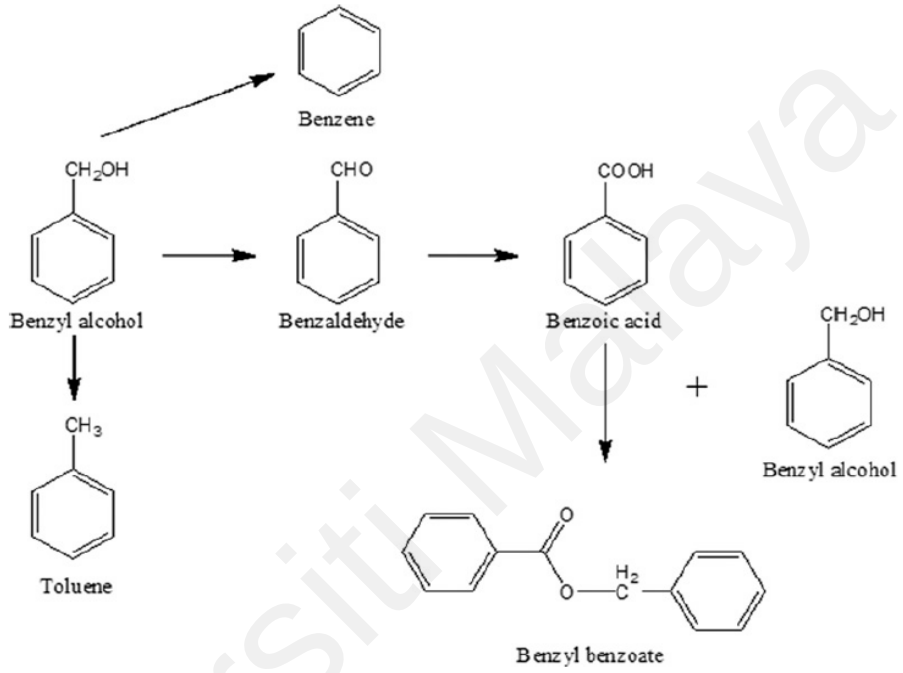

Figure 2.3: Benzyl alcohol oxidation (Villa et al., 2015) (Reproduced with permission).

Narkhede and co-workers used Mono lacunary phosphomolybdate supported on MCM-41 in oxidation of benzyl alcohol produces 28 % conversion and 90% selectivity of benzaldehyde (Nilesh Narkhede et al., 2014). It was also reported that benzaldehyde (major product) may further oxidize to benzoic acid (by-product) at temperature higher than 90 °C which resulting in higher conversion but lower selectivity towards its major product as shown in Figure 2.4. Similar studies also shown optimum temperature of 90 °C for benzyl alcohol oxidation which performed by Li et al. claimed that Pd nanoparticles supported on iron-doped SBA-15 (MagSBA) in solvent-free oxidation of benzyl alcohol using molecular oxygen under atmospheric pressure showed

excellent catalytic performance with 80% conversion and 85% selective towards benzaldehyde at low temperature (70-90 ^{o}C). Study by Hong with similar claim that the reaction temperature of 90 ^{o}C which produce 74% conversion of benzylalcohol and gave high selectivity of benzaldehyde which is 96% (Hong et al., 2014; Li et al., 2016). Wang and co-workers claimed that oxidation of benzyl alcohol to benzaldehyde provides until 50% conversion with benzaldehyde selectivity between 70-99% and benzoic acid and benzoic acid benzyl ester reported as by-product (Wang et al., 2013).

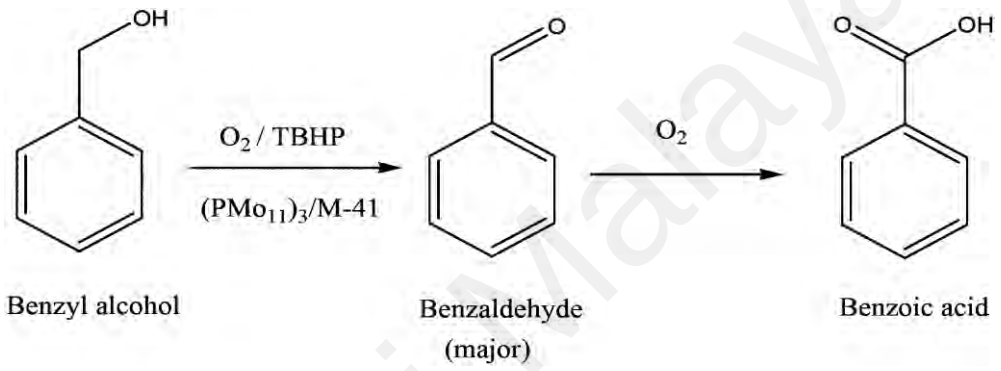

Figure 2.4: Oxidation of benzyl alcohol (Nilesh Narkhede et al., 2014) (Reproduced with permission).

Another study of liquid phase benzyl alcohol oxidation using nanoparticle gold based catalyst produced benzoic acid and methyl benzoate as major products where the conversion was reported more than 90% with 93% selectivity of methyl benzoate using Au101-based catalyst (Adnan et al., 2015). Basic condition in alcohol oxidation is known to be beneficial in removing hydrogen thus promoting to higher reaction rate (Zhu et al., 2014). The use of potassium carbonate (K_2CO_3) as base in solvent free condition of benzylalcohol oxidation increases the conversion from 2 % to 76% with 56% selectivity to benzaldehyde (Zheng & Stucky, 2007). Study by Wei and co-worker on oxidation of benzylalcohol using caesium carbonate (Cs_2CO_3) as base together with gold supported on cerium dioxide (CeO_2) as its catalyst in increasing the reaction rate to

produce 98% benzylalcohol conversion with 99% selectivity towards methyl benzoate (Wei et al., 2015).

A greener approach where absence of solvent or base were also introduced. A study by Su and co-workers using nanoparticle gold supported on the binary mesostructure Ga-Al mixed oxide were able to catalyze benzylalcohol without addition of base in the oxidation reaction which produces 98% conversion (Su et al., 2008). Another study which uses Pt/ZnO as catalyst for benzyl alcohol oxidation under base-free aqueous conditions at room temperature produces a conversion of 94 % with nearly 100% selectivity to benzaldehyde can be obtained with ambient air as an oxidant within 10 hours reaction time (Liu et al., 2018).

Benzyl alcohol oxidation using SBA-15 supported Pd catalysts reported by Liu and co-workers, claimed the catalyst was tested for three times without significant loss of activity (conversion > 96 %) under oxygen gas (Liu et al., 2017). The research group then applied other common reduced gas (H_2, air-H_2, N_2-H_2 and vacuum-H_2) to the oxidation of benzyl alcohol at 120 ^oC and reported significant increase of benzyl alcohol conversion in the first 2 hours of reaction. The catalysts produced selectivity more than 85 % benzaldehyde as main product with 15 % toluene selectivity as main side product. Table 2.2 shows a detail list of the reaction conditions in several studies on oxidation of benzyl alcohol.

Table 2.2: Oxidation of benzyl alcohol.

Catalyst	Solvent	Base	Time (hr) & Temp (^{o}C)	Oxidant	Conv%	S%	Ref
Au/UiO-66	None	K_2CO_3	10 hrs at 80 ^{o}C	O_2	53.8	54 BZL 46 Others	(Zhu et al., 2014)
MLP/MCM-41	None	None	24 hrs at 90 ^{o}C	tbhp	28	90 BZL 10 Others	(N. Narkhede et al., 2014)
Pd/MagSBA-15	None	None	9 hrs at 85 ^{o}C	O_2	71	83 BZL 17 Others	(Li et al., 2016)
Au-Pd/TiO_2	None	None	6 hrs at 90 ^{o}C	O_2	71	95 BZL 5 Others	(Hong et al., 2014)
Au/CuO_{co}	None	None	5 hrs at 80 ^{o}C	O_2	58	98 BZL 2 Others	(Wang et al., 2013)

Table 2.2, continued.

Catalyst	Solvent	Base	Time (hr) & Temp (^{o}C)	Oxidant	Conv%	S%	Ref
Au_{101}/TiO_2-untreated	MeOH	None	4 hrs at 80 ^{o}C	O_2	99	87 MB 13 BzA	(Adnan et al., 2015)
Au/ZrO_2	MeOH	Cs_2CO_3	3 hrs at 30 ^{o}C	O_2	100	99 MB	(Yu et al., 2014)
Au/β-Ga_2O_3	MeOH	None	2.5 hrs at 90 ^{o}C	O_2	90	93 MB 4 BZL 3 Others	(Su et al., 2008)
Pt/ZnO	H_2O	None	10 hrs at 26 ^{o}C	Air	94	100 BZL	(Liu et al., 2018)
Pd/SBA-15	p-xylene	None	3 hrs at 120 ^{o}C	O_2	99	90 BZL 10 Others	(Liu et al., 2017)

2.2 Gold Nanoparticles (AuNPs)

Gold is often considered the most inert of all metal but decrease in particle size to nano-sized particles demonstrates impressive catalytic activity. Studies on gold catalyst so far assumed that gold nanoparticles is presence as monodispersed layer produce high catalytic activity due to strong metal-support interaction (Miah et al., 2017). As particle size becomes smaller the surface area is increasing and hence, more active sites are accessible to the reactants to increase catalytic activity (Zhao et al., 2016). The particle size and catalytic activity of the gold catalyst are greatly influenced by the preparation methods and variable parameters. Particle size less than 10 nm is considered as the best established requirement for preparing an active catalyst (Bond et al., 2006; Chen et al., 2017; Haruta, 2011; Masatake, 2003; Takale et al., 2014; Takei et al., 2012). Introducing gold nanoparticles on the support is the first main step for the preparation method. The optimum gold particle size for oxidation of CO and catalysis was agreed to be lower than 5 nm with cautious control of the conditions of preparation (Carabineiro et al., 2015; Carabineiro & Thompson, 2007; Zanella et al., 2002).

Nanoparticles preparation is divided into 2 type which are bottom up and top down method as shown in Figure 2.5 (Jamkhande et al., 2019). Top down is the method where starting material used available in bulk material is reduced to nanoparticles by different physical, chemical and mechanical processes whereas bottom up is the method where the molecule size is increased to a certain particle size (Pacioni et al., 2015). Top-down method appears to be easy to perform but not suitable in producing nanoparticle size. Other major drawback is the changes in surface chemistry and physicochemical properties when the particle changes to nano size (Nadagouda et al., 2011).

Top down method which includes ion sputtering (Jamkhande et al., 2019; Matsuyama et al., 2020; Swihart, 2003) and laser ablation (Jafari Eskandari et al., 2020;

Simakin et al., 2004), while bottom up methods includes impregnation (Carabineiro & Thompson, 2007; Chen et al., 2016), co-precipitation (Carabineiro & Thompson, 2007; Haruta, 1997; Masatake, 2003), chemical vapor deposition (Carlsson & Martin, 2010; Hoyos-Palacio et al., 2019; Makhlouf, 2011), sol-gel (Cushing et al., 2004; Jamkhande et al., 2019; Rezaei et al., 2014) chemical reduction (Daruich De Souza et al., 2019; Razzaq et al., 2018), and deposition precipitation.

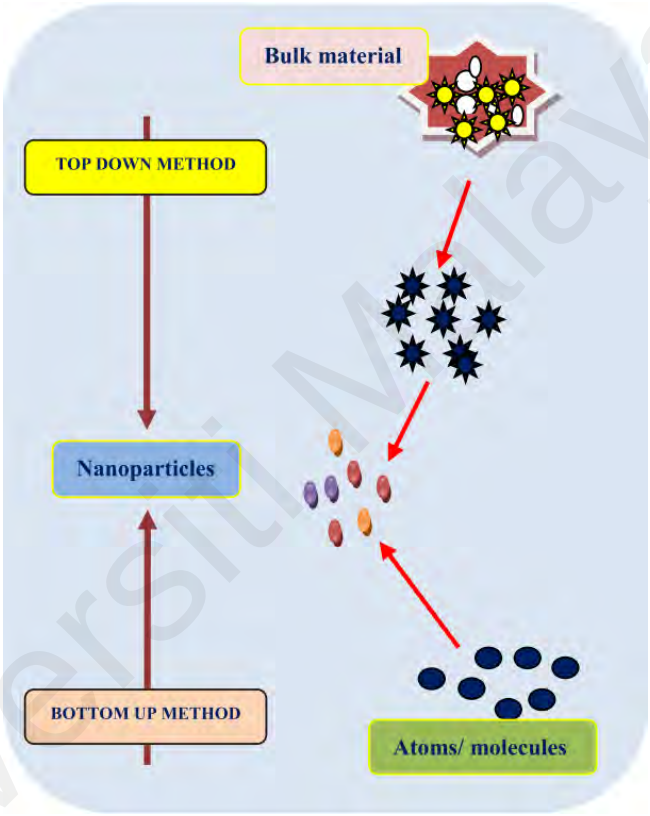

Figure 2.5: Overview of top down and bottom up method (Jamkhande et al., 2019) (Reproduced with permission).

Deposition Precipitation (DP) is known to be convenient and applicable to varieties of support materials (Wolf & Schüth, 2002) except activated carbon (Carabineiro & Thompson, 2007) and zeolite (Chen et al., 2017; Lin & Wan, 2003) due to their high isoelectric point. DP method is more convenient than co-precipitation in term of catalytic activity and producing small gold particles supported on metal oxides (Zanella et al., 2002). In the application, DP is commonly used to yield hemi-spherical structure

particle, higher dispersion with high interaction onto the support (Chen et al., 2016). DP method involves the metal precursor mixed with an aqueous suspension of the support and subsequently precipitated as hydroxide as pH is increased ideally in the range of 7-10 (Haruta, 1997, 2011; Zanella et al., 2005; Zanella et al., 2002). The support surface act as a nucleating agent and the key factor in this method is to prevent precipitation away from the support surface (Carabineiro et al., 2015; Carabineiro & Thompson, 2007; Zanella et al., 2002). The dispersion and size of gold particles is influence by the pH in the preparation of the catalyst. Above pH 6, the main species of Au in solution are transformed from $(AuCl_4)^-$ to $[Au(OH)_nCl_{4-n}]^-$ (n = 1–3) resulting lower particle size < 4 nm of calcined AuNPs while at lower values of pH, there is less hydrolysis of the Au–Cl bond (Carabineiro & Thompson, 2007; Haruta, 1997). Larger gold loading also depending on the pH at lower isoelectric point of the support that caused the surface to positively charged and capable in adsorbing more negatively charged gold species. However, high concentration of chloride on the surface can reduce the catalytic activity (Oh et al., 2002; Yazid et al., 2010). When pH values above the isoelectric point of the metal oxide, adsorption of the negatively charged $[Au(OH)_nCl_{4-n}]^-$ complex decreases rapidly therefore reducing the gold loading with less chloride formed at the catalyst surface (Carabineiro & Thompson, 2007; Oh et al., 2002; Yazid et al., 2010). Moreau and co-workers reported that pH 9 was the optimum value to TiO_2 support using deposition precipitation for CO oxidation because anionic Au complexes were formed at this pH and chloride could be removed by hydrolysis (Moreau et al., 2005).

DP using urea appeared to be better than DP in NaOH as it promotes gradual and homogeneous addition of hydroxide ion in urea (Zanella et al., 2005). Therefore, urea prevented a local increase in pH and allowed gold in solution deposited on the support surface as gold (III) precipitate, not gold (III) hydroxide (Aguilar-Tapia et al., 2016; Zanella et al., 2005; Zanella et al., 2002). Several studies shown DP with urea produce

same gold particle sizes (2–3 nm) (Chen et al., 2017; Costa et al., 2012; Fujita et al., 2016; Méndez-Cruz et al., 2011; Zanella et al., 2002). The gradual increase of pH due to urea decomposition at 80 °C change the surface charge density of the gold precipitate particles which lead to fragmentation of the particles. The method that was developed by Haruta showed higher gold loading could be achieved using urea as co-precipitator compared to NaOH (Zanella et al., 2005; Zanella et al., 2002). A list of compilation study using DP method for gold nanoparticles synthesis and its application shown in Table 2.3.

Table 2.3: DP method with particle size, gold loading material support and its application.

DP method	Catalyst	AuNP size (nm)	Au loading (wt%)	Material support	Application	Conv. (%)	Reference
DP Na_2CO_3	Au/Fe_2O_3	3 – 7	-	Fe_2O_3	CO oxidation	10	(Khoudiakov et al., 2005)
DP Urea	Au/HT	4.2	0.5 – 1.8	hydrotalcite (HT)	CO oxidation	80	(Dobrosz et al., 2005)
DP NaOH	Au/ZnO	4.5	3.5	ZnO	-	-	(Yazid et al., 2010)
DP Urea	Bimetallic Au-Cu/TiO_2	2.0	4.0	TiO_2	CO oxidation	100	(Sandoval et al., 2013)
DP NaOH	Au/Y (HY)	1.0	1.5	Proton-type zeolite Y(HY)	CO oxidation	70	(Chen et al., 2017)
DP NaOH	Au/MO_x	2.3 – 5.5	-	Metal oxide (Al_2O_3, Fe_2O_3, TiO_2, ZnO, CeO_2)	CO_2 hydrogenation	90	(Vourros et al., 2017)
DP Urea	Au/TiO_2	2.2 – 4.4	3.0 & 9.0	TiO_2 nanotube	CO oxidation	100	(Méndez-Cruz et al., 2011)
DP Urea	Au/TiO_2	2.0 – 5.6	2.0 – 7.8	TiO_2	-	-	(Zanella et al., 2005; Zanella et al., 2002)
DP Urea	Au/MgO	2.3	-	MgO	Alcohol oxidation	100	(Costa et al., 2012)
DP Urea	Au/MO_x	1.8 – 4.5	6 – 12	Metal oxides	CO oxidation	50-90	(Fujita et al., 2016)
DP Urea	Au/ZnO	1.5-7.5	0.5-8	ZnO	EB oxidation	50-70	Current work

2.3 Material Support

Gold nanoparticles have been widely studied in several material support namely activated carbon (Ghadamgahi et al., 2016), Poly (N-vinyl-2-pyrrolidone) or PVP (Tsunoyama et al., 2009), zeolite (Chen et al., 2017), mesoporous silica (Santa Barbara Amorphous also known SBA-15) (Biradar & Asefa, 2012; Martynyuk et al., 2015; Wu et al., 2013), graphene (Bahar & Ekinci, 2020; Marinoiu et al., 2020), carbon nanotube (CNT) (Jawale et al., 2014; Kaboudin et al., 2019), several metal oxides and metal hydroxides (Aguilar-Tapia et al., 2016; Chen et al., 2016; Fujita et al., 2016; Méndez-Cruz et al., 2011; Vourros et al., 2017; Zanella et al., 2002)

Poly (N-vinyl-2-pyrrolidone) or PVP stabilized gold clusters which having particle smaller than 1.5 nm appeared to have high catalytic activity in aerobic oxidation (Tsunoyama et al., 2009). It is stated that the catalyst is catalytically active due to the negative charged by electron donation from PVP. Study by Jawale and co-workers show that gold nanoparticles supported on carbon nanotube as catalyst (AuCNT nanohybrid) efficiently promotes various organic transformations. It is also mentioned that the size dependency become less significant when considering gold surface atoms only opposed to gold content (Jawale et al., 2014). A novel functionalized multi wall carbon nanotube (MWCNT) also provide efficient support for the AuNPs as it gives high conversion of 100% towards benzoic acid under 50 °C with the addition of a base (K_2CO_3) (Kaboudin et al., 2019). Synthesized SBA-15 as support for AuNPs show particle size of more than 5 nm and efficient gold loading for the ethylbenzene oxidation which give almost 90% conversion (Biradar & Asefa, 2012).

A novel study of synthesize gold nanoparticle on graphene oxide nanosheets functionalized with cationic poly-diallyldimethylammoniumchloride (PDDA) appear successful for the application of cathodic oxygen reduction reaction (ORR) electrode in

proton exchange membrane fuel cells (PEMFC) (Marinoiu et al., 2020). $AuCl_4^-$ ions attached electrostatically to the positively charge surface of graphene due to the PDDA function (Marinoiu et al., 2020). Another study of self-assembly hollow porous AuNPs on graphene oxide which uses PVP solution and hydroquinone solution that used for size control of HPAuNPs appear promising in the application of electrochemical supercapacitor applications (Bahar & Ekinci, 2020).

The use of Norit activated carbon as a support for gold nanoparticles provide a range of 1 – 3 nm gold particle size also show high catalytic activity for benzylalcohol oxidation with 100% conversion towards methyl benzoate and benzoic acid (Ghadamgahi et al., 2016). Zeolite known to be less active as a support for gold nanoparticles due to low isoelectric point of HY zeolite. However, with the pretreatment of Na^+ on the zeolite the surface charge reversed to positive thus in favour for the $AuCl_4^-$ to attached and form AuNPs (Chen et al., 2017).

Among the metal hydroxide as a support it appear that $Mn(OH)_2$ and $Co(OH)_2$ gives the highest catalytic activity towards CO oxidations (Chen et al., 2016). Metal oxides have great prospect as a material support for AuNPs and have great potential for green sustainable chemical processes (Fujita et al., 2016). There are several studies on the metal oxides as the support for AuNPs, commonly TiO_2 is used as the support due to the high interaction with the AuNPs (Haruta, 1997; Haruta, 2014; Haruta et al., 1996; Méndez-Cruz et al., 2011; Sandoval et al., 2013; Zanella et al., 2002). Some other metal oxides also provide good interaction with AuNPs such as Fe_2O_3, ZnO, ZrO_2 and Mn_2O_3 for CO oxidation except for Al_2O_3, CeO_2 and SiO_2 (Chen et al., 2016; Fujita et al., 2016; Vourros et al., 2017).

Effect of MO_x support on the catalytic activity still unclear due to the complexity of various physicochemical parameters affecting the catalytic activity and different preparation of Au/MO_x which makes difficult in making a comparison study of all MO_x (Fujita et al., 2016). Studies shown that small AuNPs (< 5 nm) and high interaction with MO_x can achieve high CO oxidation activity (Fujita et al., 2016; Haruta, 1997, 2011; Zanella et al., 2002). Fujita and co-workers introduced a metal-oxygen bonding energy of MO_x shown in Figure 2.6 as an indicator for lattice oxygen desorption as the onset catalytic activity in Au/MO_x depend on the desorption of lattice oxygen at the perimeter interface induced by deposition of AuNPs on MO_x (Fujita et al., 2016).

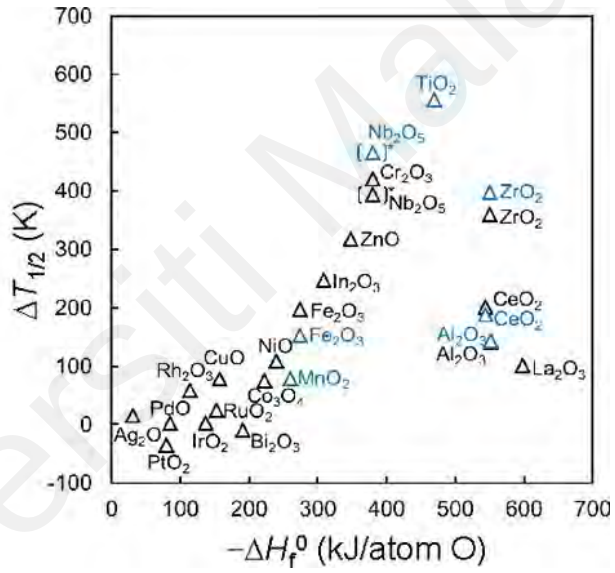

Figure 2.6: Correlation between $\Delta T_{1/2}$ and M–O bond energy per molar oxygen atom. Black triangles: Au/MOx were prepared by co-precipitation. Blue triangles: Au/MOx were prepared by deposition–precipitation (Fujita et al., 2016) (reproduced with permission).

Based on the comparative study by Fujita and co-workers it shows that the metal-oxygen binding energy for CuO, Co_3O_4, NiO, MnO_2, Fe_2O_3, In_2O_3, ZnO, Cr_2O_3, Nb_2O_5 and TiO_2 are the effective MO_x support for AuNPs by CP or DP preparation method. In addition, some MO_x have remarkable characteristic of high oxygen capacity which contribute in the high catalytic activity (Fujita et al., 2016; Wu et al., 2011). The

sequence of ordering in high oxygen capacity are Au/TiO_2>Au/ZrO_2>Au/ZnO>Au/Al_2O_3. In particular for ZnO, Cr_2O_3, and Nb_2O_5 have great potential for catalytic activity by optimization of preparation method and pretreatment condition (Fujita et al., 2016).

ZnO nanopowders as a support material for noble metal catalyst have shown promising and cost effective catalytic activity reactions as ZnO is a cheap material with excellent surface properties (Wu et al., 2011; Yazid et al., 2010). Study by Wu and co-workers Au/ZnO preparation by colloidal deposition method exhibits high catalytic activity compared with Au/Al_2O_3 and Au/MgO in Benzene-Toluene-Xylene oxidation (Wu et al., 2011).

CHAPTER 3: METHODOLOGY

3.1 Overview

This chapter highlights 3 different work stages; starting from catalyst synthesis to catalytic studies for ethylbenzene and benzylalcohol oxidation. First stage covers the preparation of gold nanoparticles on zinc oxide catalyst using deposition precipitation with urea in which the objective is to obtain gold nanoparticles with particles size less than 5nm.

Second stage covers catalyst characterization using ATR–FTIR (Attenuated Total Reflectance-Fourier Transform Infrared), X-ray Diffraction (XRD), High-resolution transmission electron microscopy (HR-TEM), X-ray Fluorescence Spectrophotometer (XRF), and Brunauner-Emmet-Teller (BET) surface area analyser. The final stage covers the catalytic studies for ethylbenzene and benzylalcohol oxidation.

3.2 Materials & Chemicals

All chemicals were of analytical grade with high purity. Acetonitrile for analysis (99.5 %) anisole (99.0 %) and benzyl alcohol (99.5 %) were purchased from Emsure Merck, urea (AR grade) from Friendemann Schmidt, phenylethyl alcohol from Acros, gold (III) chloride trihydrate and zinc oxide nanopowder from Sigma Aldrich. While other analytical standards such as benzaldehyde (99%), ethylbenzene (99%), acetophenone (99%), benzoic acid (99%) and t-BHP solution 70 wt% in water, were from Sigma Aldrich.

3.3 Experimental Method

3.3.1 Synthesis of AuNPs on ZnO

The catalyst was prepared by deposition precipitation using urea in low light condition (Perego & Villa, 1997; Zanella et al., 2002). Zinc oxide nanopowder (< 50nm) was used as the support material for gold loading. Urea ($CO(NH_2)_2$) was used as the precipitating agent that allowed the gradual and homogeneous introduction of hydroxide ion in the process, while preventing the local increase in pH and the precipitation of metal hydroxide.

Zinc oxide nanopowder (1 gram) was pre-dried at 100 °C for 24 hours prior to the addition of 100 mL aqueous solution of the gold precursor, where the amount of gold corresponds to the maximum gold loading on ZnO. The weight % of gold in 1g of ZnO were 0.254 mM (0.5 wt%), 1.015 mM (2 wt%), 2.031 mM (4 wt%) and 4.060 mM (8 wt%). The deposition of gold onto ZnO was prepared in the excess of urea, with a ratio Au: urea of 1:100. The pH of the mixture was adjusted at 7 in the excess of urea. The mixture was then separated by centrifugation at 6000 rpm for 15 minutes at room temperature. The supernatant was removed while the precipitate was dried at 100 °C for 2 hours under vacuum, prior to calcination at 300 °C for 4 hours at a heating rate of 2 °C min^{-1}. The catalyst was stored in the dark fridge at -5 °C.

Several precautions need to be taken while synthesizing the catalyst such as catalyst preparation need to be done at low light condition as it affect the degradation of the gold precursor and size of the nanoparticles (Zanella et al., 2002). Any handling with the gold precursor must be performed using glass material as it would stain the stainless-steel material since the gold could act as a catalyst to oxidize the surface of the steel by reacting with air.

3.3.2 Characterization of the catalyst

3.3.2.1 Shimadzu X-ray Fluorescence Spectrophotometer (μ-EDX 1400)

Gold loading wt% on zinc oxide was determined using x-ray fluorescence (XRF) a non-destructive analytical technique used to determine the elemental composition of materials. The measurement by the XRF on the fluorescent (or secondary) X-ray emitted from a sample when it is excited by a primary X-ray source is the main principle in determining the chemical composition of the sample (Kramar, 2017; Sperling, 2005). Each of the elements present in a sample produces a set of characteristic fluorescent X-rays ("a fingerprint") that is unique for that specific element. Based on Figure 3.1 it shows that the principle of XRF when an atom in the sample is struck with an X-ray of sufficient energy (greater than the atom's K or L shell binding energy), an electron from one of the atom's inner orbital shells is dislodged. The atom regains stability, filling the vacancy left in the inner orbital shell with an electron from one of the atom's higher energy orbital shells. The electron drops to the lower energy state by releasing a fluorescent X-ray. The energy of this X-ray is equal to the specific difference in energy between two quantum states of the electron. The measurement of this energy is determination of XRF peaks with varying intensities which are representing the concentration; meanwhile the peak energy indicates the element. Setting for XRF which include around 1g of samples and the analysis is at ambient temperature.

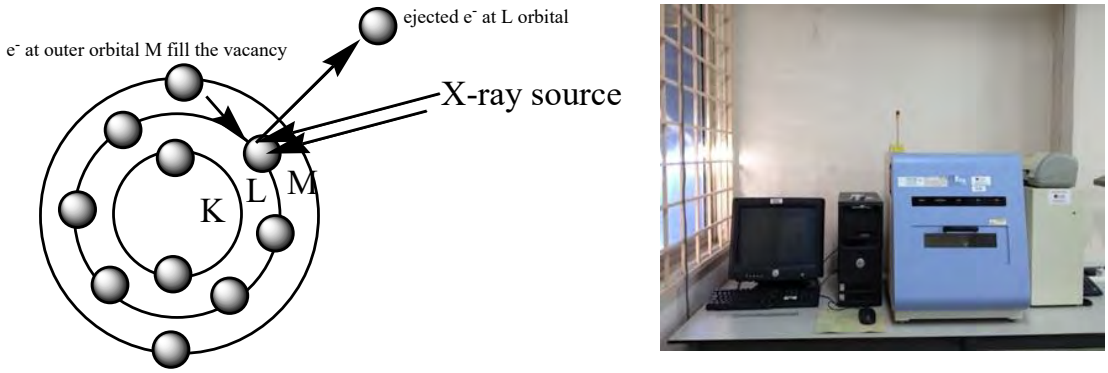

Figure 3.1: XRF principle and Shimadzu X-ray fluorescence spectrophotometer (μ-EDX 1400).

3.3.2.2 PANalytical X-ray diffraction (EMPYREAN)

X-ray diffraction (XRD) technique is one of the most widely used in materials characterization due to its capability of a non-destructive test and able to provides information on structures, phases and crystal orientation. Figure 3.2 show how diffraction of x-rays by crystal plane able to derive the lattice spacing (d) by using the Bragg's Law ($n\lambda = 2d\sin\Theta$) which Sir W.H. Bragg and his son Sir W.L. Bragg develop the XRD technique in 1913 where n is order of reflection, λ is wavelength of x-ray, d is the characteristic spacing between the crystal plane of a given specimen and Θ is the angle between incident beam and normal to the reflecting lattice plane (Chatterjee, 2001).

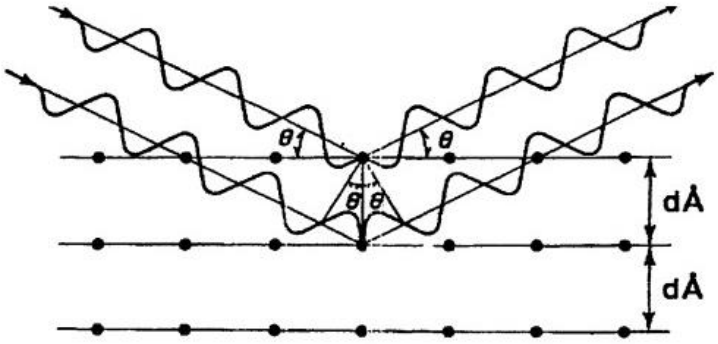

Figure 3.2: Diffraction of X-ray on crystal plane (Daily, 2021)

Identification of the XRD pattern is based on data compared with standard line patterns available for various compounds in the Powder diffraction file (PDF) database which annually updated by the International Centre for Diffraction Data (ICDD) formerly known as Joint Committee on Powder Diffraction Standards (JCPDS). As of 2019 the release of 2020 PDF have collected 1,004,568 patterns.

Interpretation of a diffractogram varies depending on one's objectives. Peak positions and intensities associated with an x-ray diffraction pattern enable qualitative analysis which appear useful for lattice constant determination and stress determination. The peak angles and profiles may further be used to determine particle size and degree of crystallization.

In this study XRD of EMPYREAN brand (PANalytical) in Figure 3.3 was used, where the lattice parameters of synthesized catalyst were determined at ambient temperature with 2-theta scan range from 20° to 90°, with a Cu Kα radiation at 40 kV and 25mA.

Figure 3.3: EMPYREAN PANalytical X-ray diffraction.

3.3.2.3 TriStar II 3020 micromeritics nitrogen thermal adsorption instrument - Brunauner-Emmet-Teller (BET) method.

BET analysis used to calculate the total surface area, pore volume and sizes of a sample. The Brunauer-Emmett-Teller (BET) method is commonly applied to calculate the specific surface area on the basis of nitrogen adsorption isotherm measurements at 77 K (Jaroniec et al., 1998). Usually, data in the relative pressure range from 0.05 to 0.3 are used. The BET model assumes multilayer adsorption of gas on the adsorbent's surface. BET method is an extension of a Langmuir model where rate of arrival of adsorption is equal to the rate of desorption. There are 5 assumptions for BET analysis which are gas molecules behave ideally, only 1 monolayer forms, all sites on the surface are equal, no adsorbate-adsorbate interaction and adsorbate molecule is immobile (Rouquerol et al., 2002). Pore determination using BET include from micropore (0.1nm-1nm), mesopore (1nm-10nm) and macropore (10nm-1500µm) (Donnet & Custodero, 2013; Rouquerol et al., 2007).

In catalysis, BET is used in determining the specific surface area of catalysts (m^2/g) calculated by the BET method, indicating the possibility of application for efficient catalytic materials. BET analysis provides precise specific surface area evaluation of materials by nitrogen multilayer adsorption measured as a function of relative pressure using a fully automated analyser. The technique includes external area and pore area evaluations to determine the total specific surface area in m^2/g which useful for the effects of surface porosity and particle size in many applications. The amount of N_2 gas adsorbed at a given pressure can be used to calculate the number of adsorbed gas molecules that would form a monolayer on the surface of the sample. Based on the known size of the adsorbate which is N_2, the surface area can be calculated. In the project TriStar II 3020 Micromeritics nitrogen thermal adsorption instrument is used in performing BET analysis.

Figure 3.4: TriStar II 3020 micromeritics nitrogen thermal adsorption instrument.

3.3.2.4 Perkin Elmer Attenuated Total Reflectance-Fourier Transform Infrared (Spectrum 400)

Infrared spectroscopy is a simple and reliable technique widely used in both organic and inorganic chemistry mainly is used in quality control and monitoring applications. Attenuated total reflectance-fourier transform infrared (ATR-FTIR) is

an infrared spectrometer equipped with ATR accessories which was performed at room temperature in the range between 450 – 4000 cm^{-1} to detect any trace of urea in the synthesized catalyst. Small amount of sample is used (approximately 0.5 g) in the analysis as it is non destructive the sample can be recovered. ATR-FTIR used in the study is Perkin Elmer Spectrum 400. The FTIR is well known for its fast, cheap and non-destructive analysis, when equipped with ATR it provide other advantages such as minimal sample preparation and analysis sample on its natural state. ATR-FTIR as shown in Figure 3.5 is a tool that has been proven to be useful in various applications. This technique is able to probe in situ single or multiple layers of adsorbed/deposited species at a solid/liquid interface (Hind et al., 2001).

Figure 3.5: Perkin Elmer attenuated total reflectance-fourier transform infrared (Spectrum 400).

In addition, ATR is often the preferred method for liquid analysis because it simply requires a drop of liquid to be placed on the crystal. Figure 3.6 shows the internal components in the ATR setup which allows the infrared radiation to enter from the bottom of the ATR base and redirected by five different mirrors before the radiation enters then exits the internal reflection element (IRE) and continues

towards the detector. This setup allows for the infrared radiation to probe molecules at the interface of the IRE. The one shown above is an image of a multiple reflection internal reflection element. It is called a multiple reflection IRE because the radiation makes more than one reflection within the element prior to exiting towards the detector. There are advantages and disadvantages of using a multiple reflection element. One of the advantages is that the user is able to observe stronger absorbance by the sample due to the multiple points that the radiation is interacting, however the disadvantage of using a multiple reflection element is that the light absorbance is hard to quantify due to scattering that occurs with each reflection. Other type of samples applicable for ATR-FTIR like multi-layered coating material, irregular hard shaped solid material, paints, plastics, free-flowing aqueous solutions, viscous liquids and even biological materials.

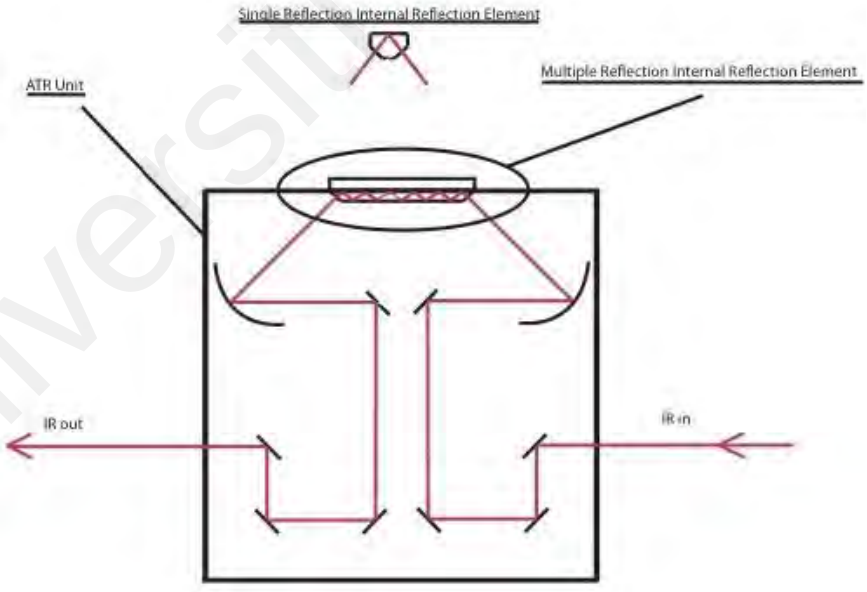

Figure 3.6: The ATR setup on FTIR ((Daily, 2021)

3.3.2.5 Jeol High Resolution Transmission Electron Microscopy (JEM 2100-F)

Image analysis on a heterogeneous catalyst always consider a compulsory in confirming the size of nanoparticle and the interaction of the nanoparticles with the

substrate. High resolution transmission electron microscopy is a powerful tool in determine the size of nanoparticles. It allows the high-resolution imaging of the crystallographic structure of a sample at the atomic scale (Ganesh Kumar et al., 2016). The use of HRTEM as imaging analysis is to determine the particle size of the synthesized gold nanoparticles on ZnO. HRTEM used in the study is from Jeol Jem 2100-F operated at 200 kV, the micrograph obtained from the HRTEM were analyse using the ImageJ software to calculate the average particle size and particle distribution. Sample preparation for the sample using the formvar carbon film on 400mesh copper grid is prepared by dilute the catalyst (5mg) in 5mL of ethanol and subject to sonication for 10 minutes before dip the copper grid in the solution (Sun & Sue, 2015). Drop method is not suitable for the sample as the catalyst move towards the edges of the copper grid which appear dense and not able to check the nanoparticles clearly. Drop method is applicable if a different type of grid is used which is the lacey carbon film coated grid. This type of copper grid much useful for ultra-small sample size and applicable for biological samples. Number of mesh in copper grid representing the number of grid, higher mesh will be useful for small size sample thus 400mesh were used. Figure 3.7 shows a HRTEM (Jeol JEM-2100F) uses the FE electron gun as its source at 200kV which is essential for ultrahigh resolution in TEM analysis. The principle in TEM analysis is where the electron passes through (transmitted) to the sample which will be detected by the electron detector. HRTEM allow to magnify images of thin sample down to atomic resolution which able to measure the lattice space (d) value of a sample and support the XRD result.

In contrast with conventional microscopy, HRTEM does not use absorption for creating images; instead the images are produce from interference in the image plane. The interaction between electron and the image plane occur independently

where the electron wave goes through the imaging system and phase change occurs (Titus et al., 2019). With this high resolution, it is possible to image crystal structures (O'Keefe et al., 1978), defects in the crystal, and individual atoms (Joshi et al., 2008).

Figure 3.7: High resolution transmission electron microscope Jeol JEM-2100F.

3.3.3 Catalysis for Oxidation of Ethylbenzene and Benzyl alcohol.

The reaction was performed in silicone gel bath which heated the ethylbenzene mixed with an internal standard of anisole using acetonitrile as solvent as shown in Figure 3.8. The mixture was added with 50mg of synthesize Au/ZnO catalyst. This reaction was continued for 24 hours at reflux temperature under constant stirring. The reaction product was then subjected to cleaning by centrifuge at 6000 rpm for 10 min. The clean and filtered supernatant was collected and undergone GC-FID analysis for quantitative analysis of oxidation products. Meanwhile, the reacted catalyst was also cleaned by washing with acetonitrile and centrifuge with same condition twice. The catalytic studies involve the effect of solvent, effect of oxidant molar ratio, effect gold loading (wt%), effect of reaction time, reaction temperature

and the catalyst weight (mg). In benzylalcohol, almost similar process condition except the weight of catalyst was 30 mg, reaction time was set at 8 hours at 80 °C.

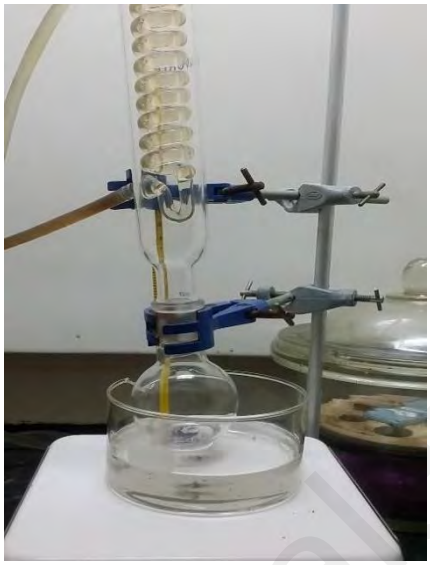

Figure 3.8: Oxidation reaction (catalysis) setup.

3.3.4 Product Analysis

3.3.4.1 Agilent Gas Chromatography Flame Ionization Detector (GC-FID)

Gas chromatography (GC) is a common type of chromatography used in analytical chemistry for separating and analysing volatile compounds based on its boiling points (Stauffer et al., 2008). A GC operates by introducing a sample via an injection port into the inlet (also called injector). Carrier gas (helium, nitrogen, argon), which is the mobile phase, passes through the inlet, and sweeps the sample onto the column, where the stationary phase is. The column is enclosed in a temperature-controlled oven as shown in Figure 3.9. The chromatographic separation takes place as the mixture travels through the column. When the separated components of the sample exit the column, they enter a detector, which provides an electronic signal proportional to the amount of eluting analytes (Hussain & Keçili, 2020).

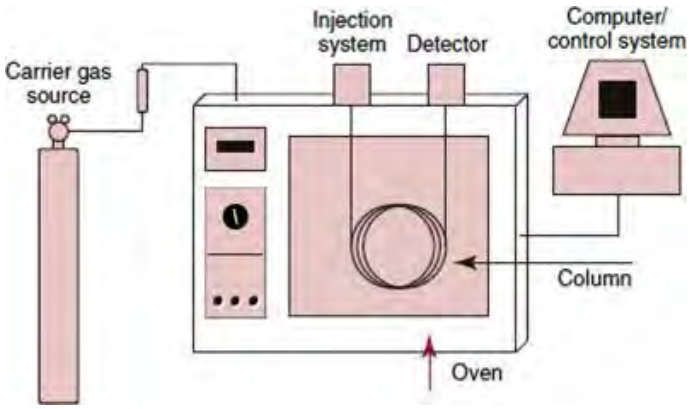

Figure 3.9: Schematic diagram of a GC (Hussain & Keçili, 2020). (Reproduced with permission).

The detector used in this study was flame ionization detector (FID). FID is very sensitive to hydrocarbons, organic compounds which contain hydrocarbon and volatile organic compounds, thus it has been extensively used in research. The operation of the FID is based on the detection of ions formed (CH+ ions and electron) during combustion of organic compounds in the hydrogen or air flame. These ions are collected and charge particles produce a measurable current flow in the detector. The comparison of peak area of analyte with the calibration curve need to be done using reference standard for an accurate quantitation. The fastest moving solute elutes the column first. As each solute elutes from the column, it enters the heated detector (FID). Several factors may affect the longer retention time (long and better separation analysis) such as analyte polarity, column phase polarity, low boiling point, low column temperature, low carrier gas flow rate and longer column. Overall gas chromatography provides the advantages of high sensitivity, high accuracy, and precision, in addition to simple operation, and it is suitable for batch analysis. However, the key to whether the components can be separated is the chromatographic column and optimizing the temperature programming. Whether the components can be identified after separation is based on the detector, so the

separation system and the detection system are the core of the instrument (Li & Liu, 2019).

Product analysis was run using Agilent Gas Chromatography Flame Ionization Detector (GC-FID) with HP-5 semi-polar column (composition 5 % Phenyl 95 % dimethylpolysiloxane) as shown in Figure 3.10. The inlet was set to a split mode with 50:1 ratio at 250 °C. Carrier gas used is hydrogen with flowrate at constant linear velocity at $40cms^{-1}$. Table 3.1 show the temperature programming in analysing for ethylbenzene and benzylalcohol oxidation product with total runtime of 19.2 minutes. Table 3.2 show the retention time for all compound used in the experiment.

Figure 3.10: Agilent 7890A series GC-FID.

An overlap may occur between chlorobenzene retention time with ethylbenzene, thus internal standard for ethylbenzene used was anisole while for benzylalcohol oxidation the internal standard used was chlorobenzene as it does not have overlap in retention time with the other related compound. Table 3.2 show the retention time for all compound used in the experiment together with Figure 3.11 which an example of ethylbenzene oxidation product analysis chromatogram.

Table 3.1: Temperature programming setting for oxidation product.

Rate (°C/min)	Temp. (°C)	Hold time (min)
-	60	2
15	150	3
25	280	3

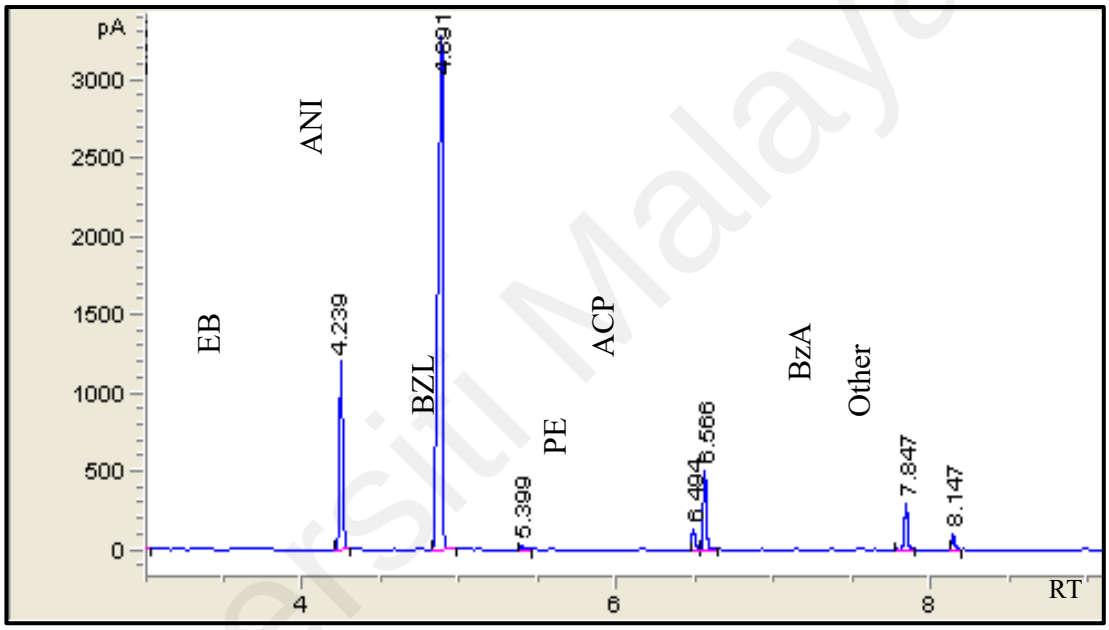

Figure 3.11: Chromatogram for ethylbenzene oxidation reaction.

Table 3.2: Retention time for oxidation of ethylbenzene and benzyl alcohol in GC-FID.

Standard	RT (min)	BP (°C)	Molar mass (g/mol)	Density (g/mL)
Acetonitrile (ACN)	2.516	82	41.05	0.786
t-BHP	3.127	37	90.12	0.935
Ethylbenzene (EB)	4.239	136	106.17	0.8665
Chlorobenzene (CB)	4.515	131	112.56	1.11
Anisole (ANI)	4.891	154	108.14	0.995
Benzaldehyde (BZL)	5.399	178	106.12	1.04
Benzyl Alcohol (BA)	6.355	205	108.14	1.04
1-phenylethanol (PE)	6.494	204	122.16	1.012
Acetophenone (ACP)	6.566	202	120.15	1.03
Benzoic Acid (BzA)	7.847	249	122.12	1.27

A series of working standard solutions 0.025 M, 0.050 M, 0.075 M, 0.100 M, 0.125 M, 0.150 M, 0.175 M and 0.200 M with addition of 0.2M of anisole as internal standard were prepared using an intermediate standard 0.25 M of ethylbenzene from a stock standard 99% Ethylbenzene (Sigma Aldrich). Acetonitrile was use as the solvent for mark up until calibration mark of the volumetric flask (25 mL). Calibration curve for benzyl alcohol was prepared with intermediate standard of 0.1 M to form a series of standard solution of 0.004 M, 0.008 M, 0.012 M, 0.016 M and 0.020 M with the addition of 0.2 M of chlorobenzene as internal standard (shown in Appendices).

Calibration curve for product of the reaction also were prepared from an intermediate standard of 0.10 M acetophenone, benzaldehyde, 1-phenylethanol and methylbenzyl acetate to form a series of standard solutions of 0.01 M, 0.02 M, 0.03 M, 0.04 M and 0.05 M, followed with the addition of 0.2 M anisole to each standard.

CHAPTER 4: RESULTS & DISCUSSION

4.1 Characterization on Au/ZnO Catalyst

The synthesize catalysts were characterized by several instrument such as XRF, XRD, BET, ATR-FTIR and HRTEM. Table 4.1 shows the summary of the characterization test.

Table 4.1: XRF gold loading, BET surface area, pore size, pore volume and HRTEM average gold particle size.

Catalyst	Au loading (wt%)	BET surface area (m^2/g)	Pore volume (m^3/g)	Pore size (Å)	Particles Size (nm)
ZnO (uncalcined)	0	22.31	0.031	55.38	-
ZnO (calcined)	0	10.56	0.035	132.72	-
0.5 wt% Au/ZnO (calcined)	0.4	12.78	0.064	201.36	1.59 ± 0.25
2.0 wt% Au/ZnO (calcined)	1.9	14.54	0.070	191.24	2.31 ± 0.42
4.0 wt% Au/ZnO (uncalcined)	3.7	26.68	0.032	48.56	1.71 ± 0.33
4.0 wt% Au/ZnO (calcined)	3.4	16.20	0.073	179.98	2.85 ± 0.62
4.0 wt% Au/ZnO (spent)	3.1	19.49	0.059	120.64	7.48 ± 1.93
8.0 wt% Au/ZnO (calcined)	7.1	18.39	0.090	194.63	3.33 ± 0.56

4.1.1 Attenuated Total Reflectance-Fourier Transform Infrared (ATR-FTIR)

Figure 4.1 shows the FTIR spectra for (a) support material ZnO and various gold loading Au/ZnO (b) 0.5 wt%, (c) 2.0 wt%, (d) 4.0 wt%, (e) 8.0 wt%, (f) urea sol, (g) uncalcined 4.0 wt% and (h) spent 4.0 wt%. ZnO peaks are identified at 830 cm^{-1} (Zn-OH), 505 cm^{-1} (Zn-O), 1500 cm^{-1} (C=O) and a double peak at 1395 cm^{-1} (CH_2) (Ismail et al., 2016; Kołodziejczak-Radzimska et al., 2012), which are typical of the different amounts of Au/ZnO i.e. 0.5 wt%, 2.0 wt%, and 8.0 wt% with similar transmittance intensities. However, the (d) calcined Au/ZnO 4 wt%, (g) uncalcined 4 wt% Au/ZnO and (h) spent 4 wt% of Au/ZnO show smaller intensities because these catalysts were freshly analysed while the others were stored for 24 hrs in a refrigerator (5 °C). The FTIR spectrum also shows no peaks for the uncalcined 4 wt% Au/ZnO catalyst (g) and spent 4 wt% Au/ZnO (h). It can be concluded that the catalysts were free from traces of urea with the absence of N-H peak (~3300 cm^{-1}) after the synthesis (Gangopadhyay et al., 2015). After a period of time the catalyst stored in a refrigerator and exposed to atmosphere the catalyst tend to absorb moisture and other impurities which shown in spectra (b), (c) and (e). This however, not significantly affecting the conversion of the EB which shown in Table 4.2 where 2.0 wt% Au/ZnO (fresh calcined) and 2.0 wt% Au/ZnO (stored 8 months) shows a drop of 3% in conversion.

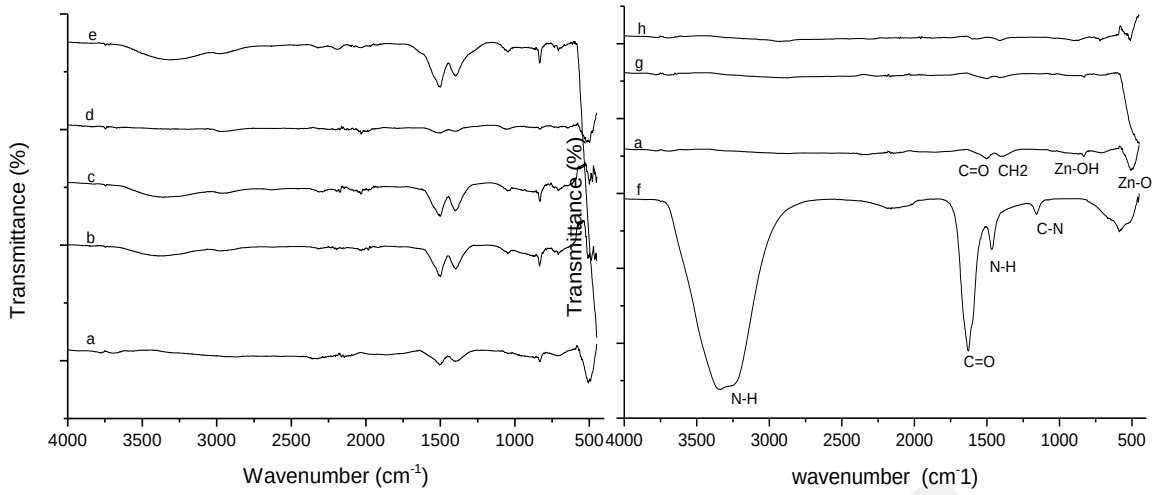

Figure 4.1: FTIR spectrum for (a) support material ZnO and various gold loading Au/ZnO (b) 0.5 wt%, (c) 2.0 wt%, (d) 4.0 wt%, (e) 8.0 wt%, (f) urea sol, (g) uncalcined 4.0 wt% and (h) spent 4.0 wt%.

4.1.2 X-ray Fluorescence Analysis (XRF)

Gold loading wt% on zinc oxide was determined using x-ray fluorescence (XRF) to quantify the elemental composition of a material. Based on Table 4.1, it proves that maintaining the pH below the isoelectric point (IEP) of ZnO (pH 9.78) able to achieve almost complete deposition to the support (Yazid et al., 2010). The spent 4 wt% Au/ZnO shows a decreased of 0.9 wt%. This may due to the leached out of metal during the reaction and washing of the recycle catalyst. Study by Zanella *et al.* (Zanella et al., 2005) and Haruta *et al.* (Haruta *et al.*, 1996) reported that larger particle sizes could be produced when the pH is less than 7. The smaller presence of Au at low pH was due to the hydrolysis of $AuCl_4^-$ precursor which makes it difficult for the deposition of gold NPs on zinc oxide. When the solution pH was higher than the IEP of metal oxides, the $AuCl_4^-$ precursor could not interact with the metal oxide surface due to the surface charge repulsion. This results in the leaching of the unreacted gold into the solution thus producing lower gold loadings (Tsubota *et al.*, 1995; Zanella *et al.*, 2005; Zanella *et al.*, 2002). Nevertheless, the dropwise addition

of urea gradually increases the pH of the gold precursor (~pH 2) to pH 7 for increased gold loadings. At the same time, the sudden increase of high concentration of urea with the gold salt could lead to the fulmination of gold (Dimitratos *et al.*, 2006). The presence of light decreased the Au wt%, as light illumination is known to decompose the gold precursor (Zanella *et al.*, 2002).

4.1.3 X-ray Diffraction Analysis (XRD)

The XRD diffractograms of ZnO (a), 2.0 wt% Au/ZnO (b), 4.0 wt% Au/ZnO (c), 8.0 wt% Au/ZnO (d) and spent 4wt% Au/ZnO (e) were shown in Figure 4.2. The diffractograms were compared with the standard database of the International Centre for Diffraction Data (ICDD). Figure 4.2 shows ZnO peaks (#) at 2θ = 32°, 34°, 36°, 47°, 56°, 63°, 66°, 68°, 69°, 72°, 77°, 81° and 90° is attributed to the (100), (002), (101), (102), (110), (103), (200), (112), (201), (004), (202), (104) and (203) planes respectively, which are similar to the results of other literatures (Akhtar et al., 2012; Perumal et al., 2016; Yazid et al., 2010). Figure 4.2 (c) show similar ZnO peaks as 4.2 (a) with no Au peaks are found as the Au is present in nanoparticle size. For crystallite sizes below 100 nm, line broadening occurs due to incomplete destructive interference in scattering directions where the x-rays are out of phase (Chatterjee, 2001). Ndolomingo et al. stated that XRD could not detect the presence of Cu and Au in the catalyst, as it was below the detection limit of 5 wt% of elemental Au (Ndolomingo & Meijboom, 2017).

The presence of gold with higher gold loadings could be detected at 38° shown in Figure 4.2 (d), where the small slope at this theta degree increases for loadings greater than 8.0 wt% Au/ZnO. Au peaks (*) are observed in Figure 4.2(e) after the oxidation reaction with gold peaks are observed at 2θ = 38°, 44° and 65° corresponds to the

Miller indices of (111), (200) and (220) possibly due to the agglomeration of gold particle. The nanoparticle size of Au will be discussed further in sub-section of HRTEM below. The low presence of gold in low gold loadings was due to the smaller size of the gold nanoparticle (< 5nm) which was confirmed from the HRTEM analysis. However, the ZnO diffraction peaks had higher intensity after calcination compared to the uncalcined ZnO as shown in Figure 4.3 as the particles were more crystalline due to calcination (Al-Hada et al., 2014). The higher intensity in the XRD diffractograms corresponds to a higher degree of crystallinity with lower surface area (Stacey et al., 2009). This is the reason for the larger surface area of uncalcined ZnO (m^2/g) compared to the calcined ZnO, as shown in Table 4.1.

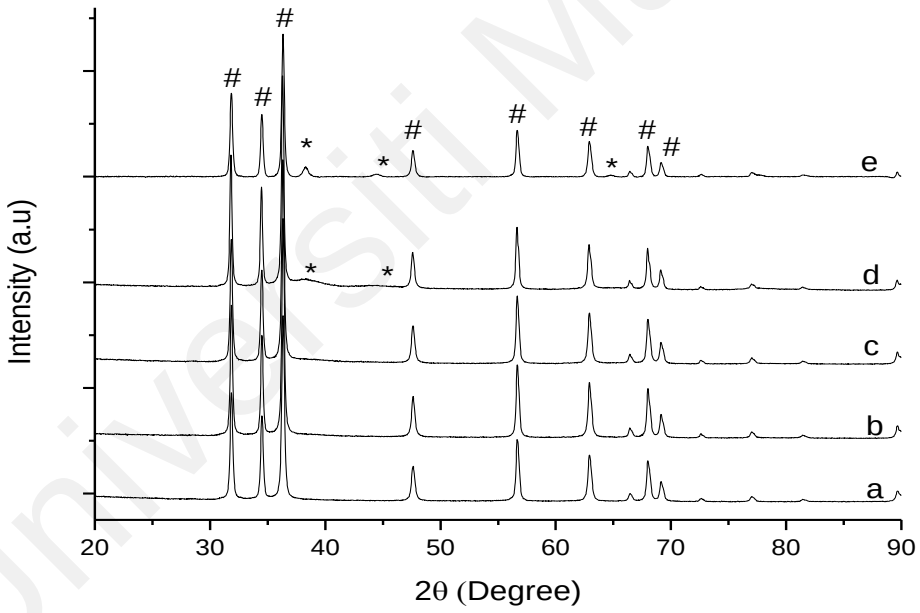

Figure 4.2: XRD diffractogram for (a) support material ZnO and various gold loading on zinc oxide (b) 2.0 wt%, (c) 4.0 wt%, (d) 8.0 wt%, (e) Spent 4.0 wt% and diffractogram of uncalcined and calcined ZnO.

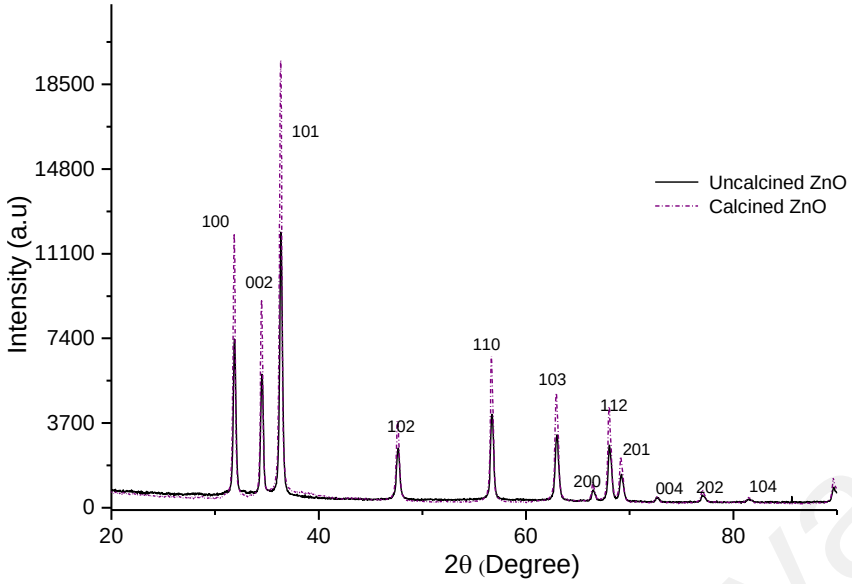

Figure 4.3: Comparison peak intensity on uncalcined and calcined ZnO.

4.1.4 Brunauner-Emmet-Teller (BET)

Figure 4.4 show the corresponding pore size distributions for (a) ZnO, (b) Uncalcined 4 wt% Au/ZnO and (c) Calcined 4 wt% Au/ZnO. Apparently, the isotherm reveals a clear hysteresis loop type IV when the relative pressure is in a certain range. This illustrates a narrow pore size distribution of ZnO supports, uncalcined and calcined Au/ZnO catalysts.

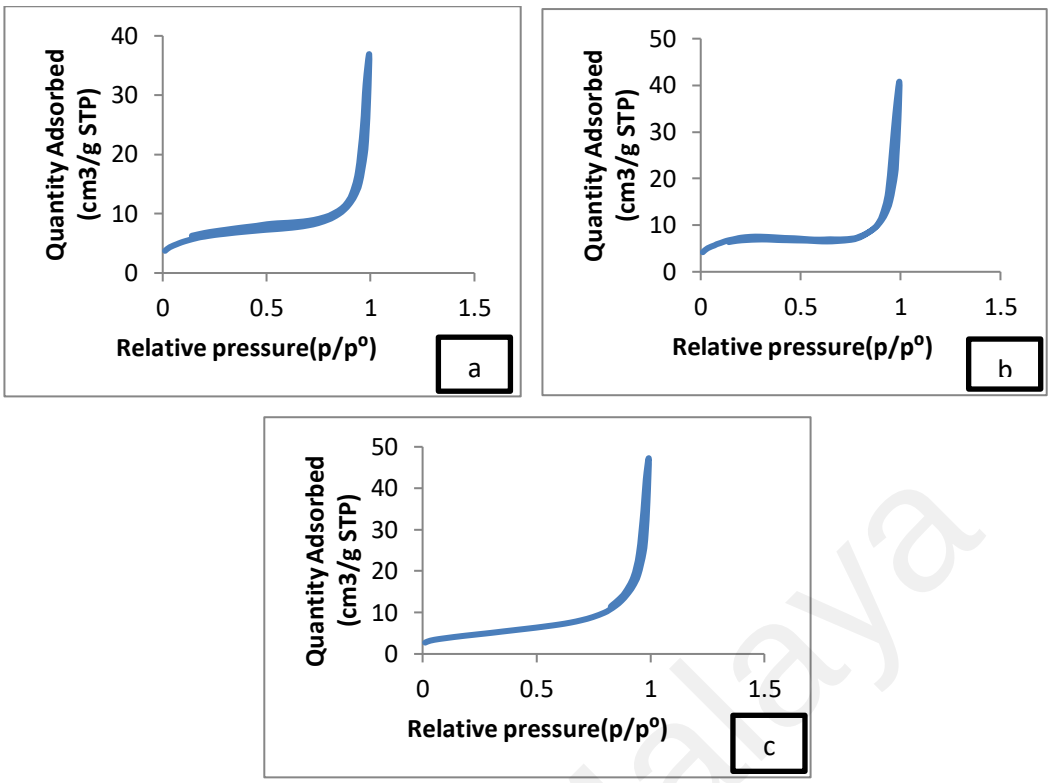

Figure 4.4: Type IV adsorption isotherm of (a) ZnO, (b) uncalcined 4 wt% Au/ZnO and (c) calcined 4 wt% Au/ZnO.

The BET result as stated in Table 4.1 above shows the variance in the surface area, pore size and pore volume of various gold loadings on zinc oxide. It is observed the deposition of calcined gold on ZnO support shows higher total surface area (m^2/g), pore size (Å) and pore volume (m^3/g) compared to calcined ZnO support. This similar finding was reported by Alabbad et al. as gold and silver metals showed higher surface area and pore volume when deposited on metal oxide (Alabbad et al., 2014; Ismail et al., 2016). Based on Table 4.1 uncalcined ZnO and uncalcined 4 wt% Au/ZnO show a reduction of surface area after calcination from 22.32 m^2g^{-1} to 10.56 m^2g^{-1} (ZnO) and 26.68 m^2g^{-1} to 16.20 m^2g^{-1} (4 wt% Au/ZnO). This indicate that the sintering proceeded drastically and the process of crystallization started to take place by the calcination process which also corresponding to the XRD results shown in Figure 4.3 (Hua, 2021). Table 4.1 shows that the AuNPs particles size increases as the metal loading (wt%) increased. This due to the higher tendency of AuNPs to agglomerates with each other and resulting an increase to the BET surface area as well as the pore volume. It is noted

the surface area of spent 4wt% Au/ZnO catalyst at 19.49 m^2g^{-1} is slightly higher than calcined 4wt% Au/ZnO catalyst at 16.20 m^2g^{-1} as it is also due to an increased in AuNPs size (7.48 ± 1.93 nm).

4.1.5 High Resolution Transmission Electron Microscopy (HRTEM)

The TEM images of all gold loadings in Figure 4.5 show uniform mesoporous structures (2-50 nm) with some of the images consist of large dark spots since they are oriented parallel to the zone axis (Bragg contrast). Another factor is the overlapping of the powder catalyst at the back of the copper grid during the sample preparation in the TEM analysis which blocks the beam thus showing a darker contrast in the image. Nevertheless, the AuNPs is visible and the sizes could be measured by the ImageJ software. Figure 4.6 is the TEM image of the uncalcined 4 wt% Au/ZnO which shows the dispersion of AuNPs on ZnO, with average particle size at 1.7 nm. After calcination, the average particle size of AuNPs is slightly bigger at 2.8 nm in Figure 4.7. The freshly synthesized Au/ZnO catalyst at different gold loadings show well dispersion AuNPs with an average particle size smaller than 3 nm, after calcination in Figure 4.8, 4.9 and 4.10. As the gold loading is increased, the void between the particles becomes smaller, hence has a higher tendency for fast agglomeration. This is in agreement with the study by Wang *et al*., where the size of AuNPs over the metal support is between 1-5 nm with a narrow size distribution (Wang et al., 2006). The shape of the AuNPs on the surface of ZnO is almost hemispherical, indicating a strong metal-oxide interaction which could enhance the catalytic activity (Yesmurzayeva et al., 2015). The smaller size of the AuNPs in the uncalcined and calcined samples is the main reason for the absence of gold peaks in the XRD diffractogram. The Au peaks could only be detected by XRD when the size of Au is larger than 5.0 nm, as in the spent catalyst which shown in Figure 4.11.

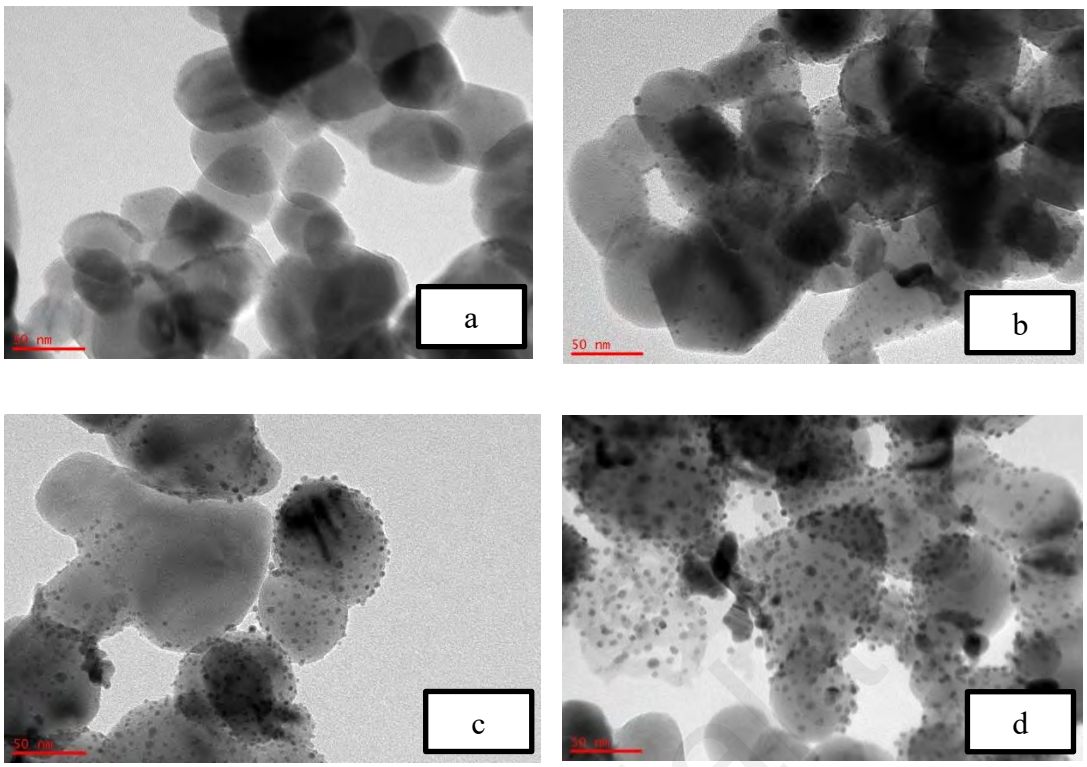

Figure 4.5: Calcined gold on zinc oxide for various gold loading at 50 nm scale images with 200kV (a) 0.5 wt%, (b) 2.0 wt%, (c) 4.0 wt% and (d) 8.0 wt%.

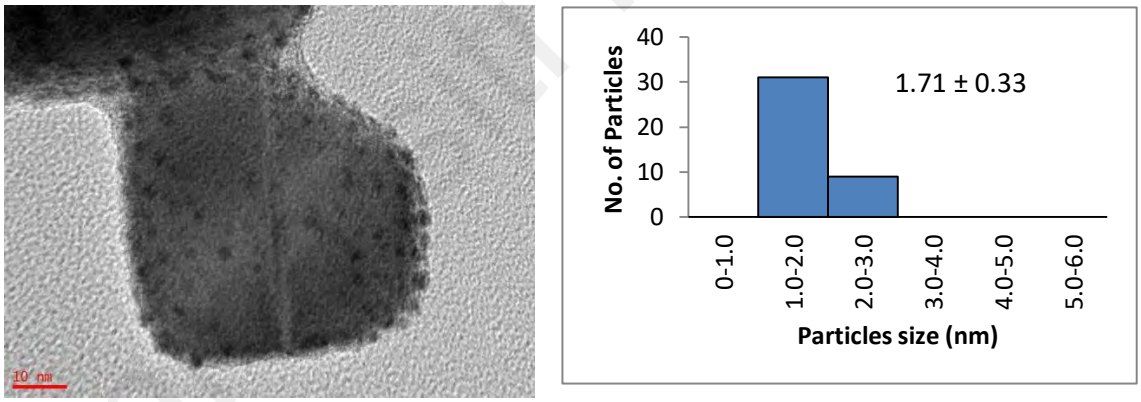

Figure 4.6: TEM image at 200kV and 10 nm scale of uncalcined 4 wt% Au/ZnO.

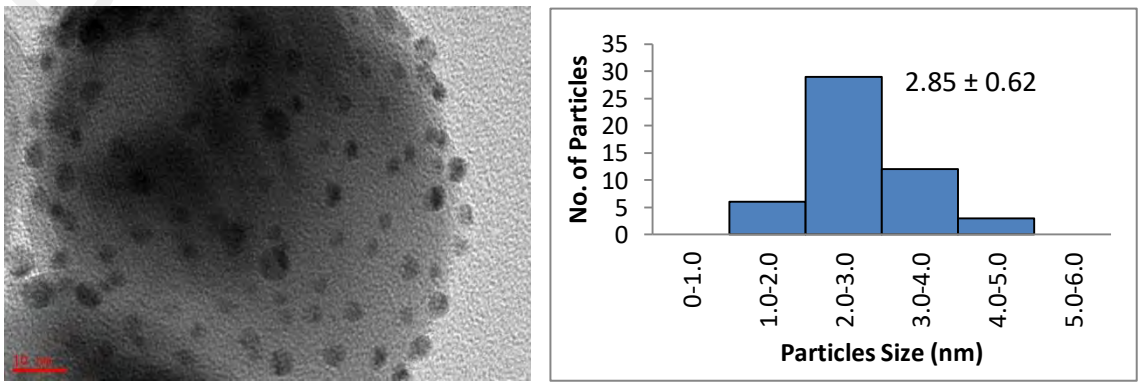

Figure 4.7: TEM image at 200kV and 10 nm scale of calcined 4 wt% Au/ZnO.

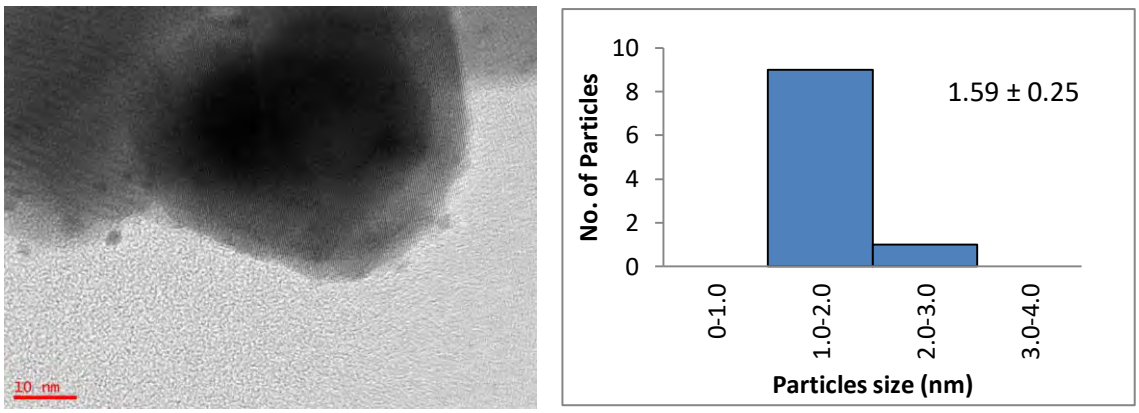

Figure 4.8: TEM image at 200kV and 10 nm scale of calcined 0.5 wt% Au/ZnO.

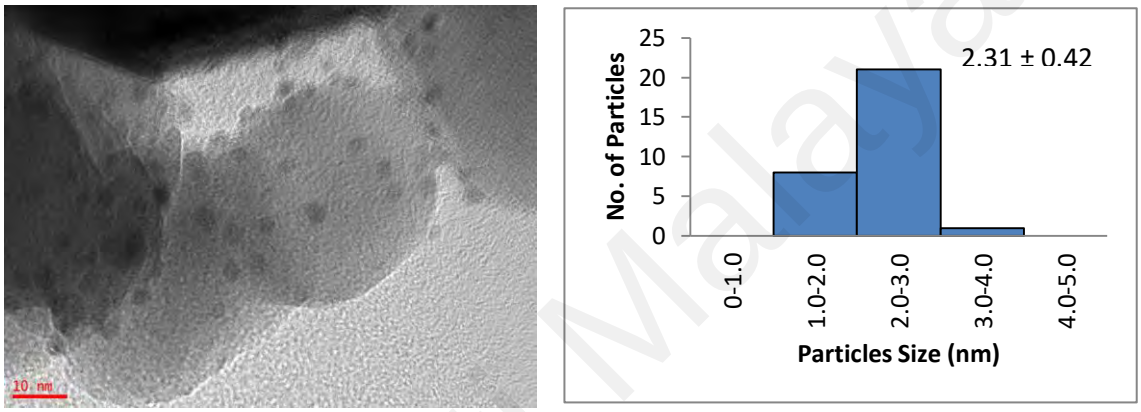

Figure 4.9: TEM image at 200kV and 10 nm scale of calcined 2.0 wt% Au/ZnO.

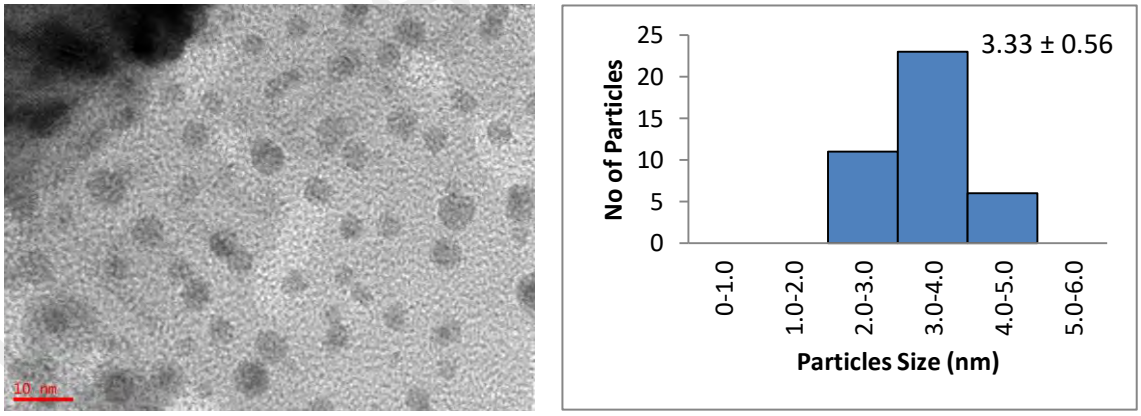

Figure 4.10: TEM image at 200kV and 10 nm scale of calcined 8.0 wt% Au/ZnO.

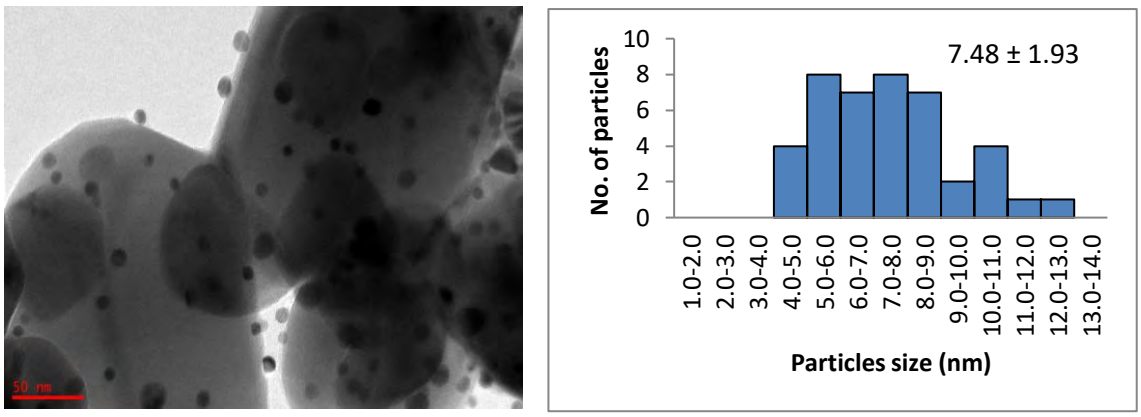

Figure 4.11: TEM image at 200kV and 50 nm scale of spent 4 wt% Au/ZnO.

4.2 Catalytic Studies and Reaction Pathway on Ethylbenzene Oxidation

The oxidation of ethylbenzene with TBHP undergoes a radical mechanism where the catalyst (Au/ZnO) catalyzed reaction goes through radical intermediates (Biradar & Asefa, 2012). The electron-deficient metal ion in the catalyst induces the adsorption of the lone pair of electrons with the remote oxygen atom in the TBHP to activate the O–O bond in the TBHP molecule which produce tert-butoxy radical (t-BuO˙) and tert-butylperoxyl radical (t-BuOO˙). In the meantime, tert-butoxy radical (t-BuO˙) also will remove benzylic hydrogen of ethylbenzene (EB) to form 1-phenylethyl radical. Immediately the tert-butylperoxyl radical (t-BuOO˙) and 1-phenylethyl radical will combine to form 1,1-dimethylethyl-1-phenylethyl peroxide. This intermediate will then undergo decomposition-abstraction where the O-O bond will break to form 1-phenyl ethoxy radical due to its low bond dissociation energy similarly like TBHP (Tang et al., 2020). The t-BuO˙ then abstracts the hydrogen from 1-phenyl ethoxy radical to produce acetophenone (ACP). Most of the byproducts of the reaction forms t-BuOH (Tang et al., 2020). Benzaldehyde (BZL) also form from a similar mechanism and benzoic acid (BzA) is produce by further oxidation of benzaldehyde (JamJam et al., 2019; Ji et al., 2021). Formation of 1-phenylethanol (PE) is associated with the concentration of free 1-phenyl ethoxyl radical, whereby the radical will remove hydrogen atom from

ethylbenzene and produce the same intermediate. Figure 4.12 shows a proposed reaction pathway for ethylbenzene oxidation with gold nanoparticles on zinc oxide and TBHP as the oxidant under reflux.

The reaction also produces another unknown compound detected by the GC which appeared at later retention time (8.147 min) as shown in Figure 3.11. There is possibility that unknown compounds as shown in Figure 4.13 were possibly phenyladehyde, phenylethyl benzoate or 1-phenyl-ethylhydroperoxide according to several research groups (Mo et al., 2020; Shi et al., 2014; Zhang et al., 2017).

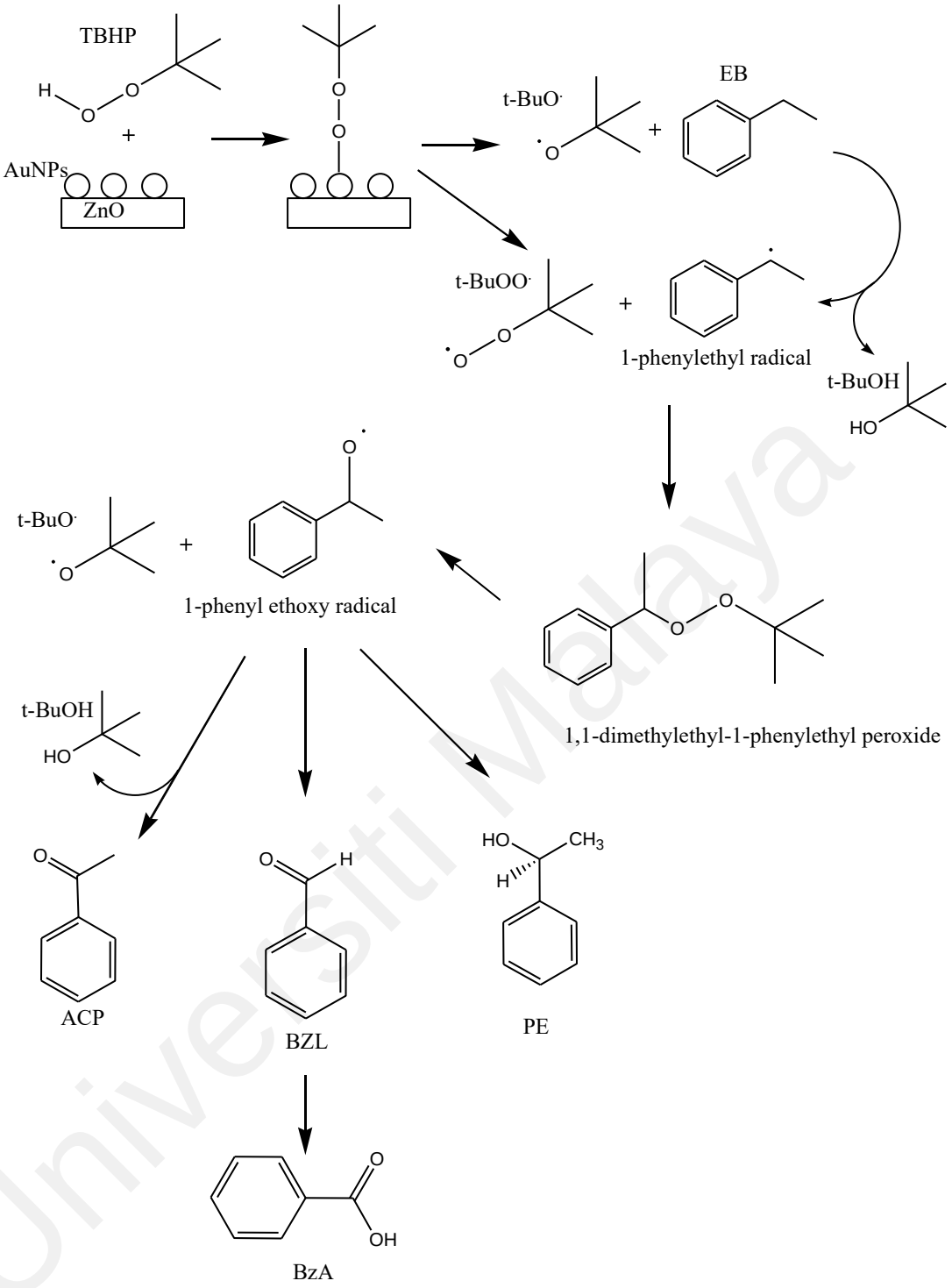

Figure 4.12: Proposed reaction pathway for ethylbenzene oxidation with gold nanoparticles on zinc oxide and TBHP as the oxidant under reflux.

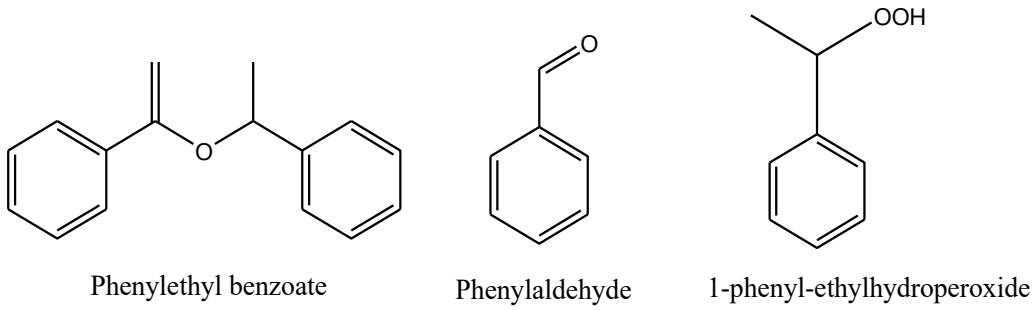

Figure 4.13: Possible unknown compounds.

4.2.1 Control Reaction

The ethylbenzene oxidation reaction without catalyst was tested using standard process condition. The control reaction showed 20.1 % conversion 20.9% selectivity towards acetophenone after 24 h of reaction even though in the absence of catalyst and material support as shown in Table 4.1. However, the presence of TBHP which play the role in the conversion of EB where the possible homolytic thermal decomposition of TBHP to form t-BuO˙ and HO˙ radicals and proceed with the same mechanism shown in Figure 4.12 (JamJam et al., 2019; Tang et al., 2020).

There was not much different with addition of material support in the reaction with the absence metal catalyst (gold nanoparticle). The material support was not directly affecting the dehydrogenation step but affects the adsorption, activation, and transfer of oxygen, which consequently improve catalytic activity (JamJam et al., 2019). Metal oxide as a support holds a higher abundance of oxygen vacancies, which contributes to the short-lived oxygen transfer O^{2-} (Chen et al., 2011). In the presence of gold on ZnO it significantly increased the ethylbenzene conversion as well as its products.

4.2.2 Effect of Calcination

The catalyst should be freshly calcined before reaction to prevent the decomposition and agglomeration of Au due to the presence of moisture and oxygen (Alabbad et al., 2014; Du et al., 2014; Zanella et al., 2002). It is observed in Table 4.2 the calcined 4 wt% Au/ZnO shows better catalytic activity compared to the uncalcined catalyst which could be due to the increased crystallinity of ZnO (Riaz et al., 2015). This postulate was supported with XRD diffractogram earlier which showed an increase in the crystallinity of ZnO support after the calcination step. Jain *et al*. reported that the increase in crystallinity enhances the support reduction properties and the degree of metal-support interaction, thus improving the catalytic activity (Jain et al., 2005). The nanoparticle size observed from TEM analysis is one of the main reasons for the high performance of the catalytic material (Biradar & Asefa, 2012; Masatake, 2003; Zanella & Louis, 2005). Nevertheless, AuNPs (Figure 4.6) for 4 wt% uncalcined Au/ZnO shows lower conversion of ethylbenzene compared to the 4 wt% calcined Au/ZnO with larger AuNPs size. This was probably due to the loosely held gold on the support material (ZnO) and Au metal was not completely activated. According to Zanella *et al*. calcination was required to reduce Au^{3+} to Au^{0}, even though thermal treatment could lead to larger particle sizes, provided that the particle growth is not drastic (Zanella & Louis, 2005). The reduction of Au^{3+} to Au^{0} could be observed from the colour change to dark purple which is due to the plasmon resonance at ~550 nm (Kamat, 2002). From the BET results in table 4.1, it can be observed that the calcination of 4wt% Au/ZnO decreases the surface area thus raising the demand for pore volume, pore size and the degree of crystallinity. Therefore, the calcination process plays an important role in the activation of gold nanoparticles by removing a significant amount of precursor residues on the catalyst, which exposes the AuNPs surface for enhanced catalytic performance.

Table 4.2: Conversion of ethylbenzene with product selectivity under standard conditions.

Catalyst	EB Conversion (%)	Selectivity (%)				
		BZL	PE	ACP	BzA	Other
No catalyst	20.1	4.9	5.5	20.9	63.2	5.5
ZnO (a)	20.6	0	5.8	18.5	77.3	0
ZnO (b)	16.7	2.2	7.1	27.2	54.8	8.7
4wt% Au/ZnO (a)	40.0	4.6	8.3	23.6	50.1	13.4
4wt% Au/ZnO (b)	54.6	2.0	15.9	49.0	26.0	7.1
4wt% Au/ZnO (c)	23.6	0	5.6	22.8	71.6	0
4wt% Au/ZnO (d)	26.3	0	15.2	84.8	0	0
0.5wt% Au/ZnO (b)	20.0	0	7.9	25.3	58.0	8.8
2.0wt% Au/ZnO (b)	24.4	0	12.6	35.9	48.1	3.4
2.0wt% Au/ZnO (e)	21.8	0	12.3	34.0	49.9	3.8
3.0wt% Au/ZnO (b)	38.0	2.9	19.5	42.9	28.5	6.1
8.0wt % Au/ZnO (b)	71.3	1.9	20.9	51.6	23.3	2.4

(a) Uncalcined catalyst (b) Calcined catalyst (c) Spent/recycled catalyst (d) Catalyst without tBHP (e) Catalyst stored up to 8 months in refrigerator

*standard condition: 50 mg catalyst added to 0.2M ethylbenzene, 0.2M internal standard, 0.2M tBHP in 5 mL volume with ACN as solvent at 100 °C for 24 hours.

4.2.3 Effect of Reaction Time

The effect of reaction time on the oxidation of EB is shown in Figure 4.14. The conversion increased linearly from 4 hours to 24 hours reaction. However, the reaction was not able to continue further than 24 hours as solvent and substrate were completely dried. Therefore, the sample retrieval from the flask was not possible. It is suggested that the set-up of the reaction would to be improved to ensure minimal solvent and substrate lost during reaction even after 24 hours. The selectivity of ACP increases from 4 hours to 8 hours before the result shows constant selectivity at 16 and 24 hours.

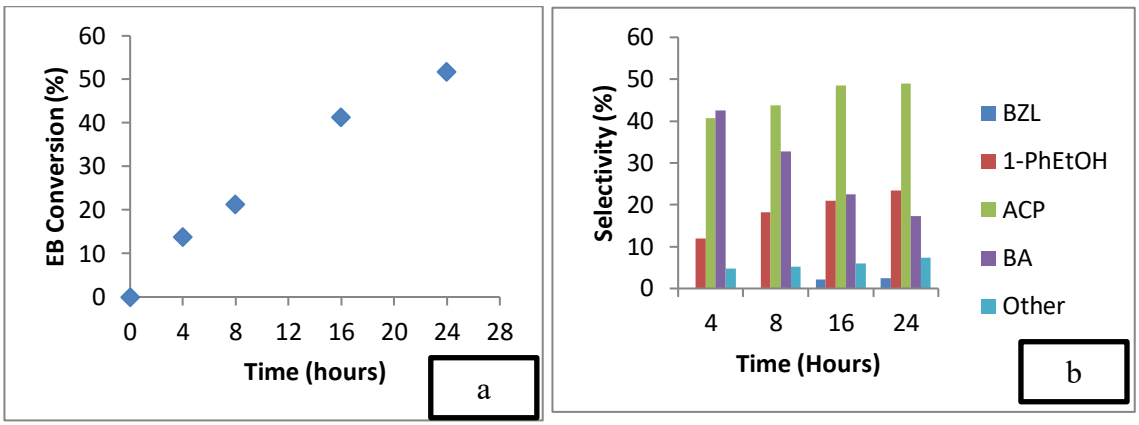

Figure 4.14: Effect of time for conversion of 0.2 M ethylbenzene oxidation (a) and product selectivity (b) using 50 mg of 4 wt% Au/ZnO at 100 °C with 1 mmol of TBHP.

4.2.4 Effect of Solvent

To optimize the reaction conditions, the selection of a suitable solvent was also studied. Figure 4.15 shows the effect of solvent towards the oxidation of ethylbenzene in the presence of 4wt% Au/ZnO catalyst in reaction temperature at 100 °C for 24 h. The solvents tested in this study were acetonitrile, tetrahydrofuran (THF), ethyl acetate and toluene. Acetonitrile shows the highest conversion of 54.6 % while THF provide 33.7 % of conversion. Toluene shows the lowest conversion while ethyl acetate fared slightly better. The decrease in the catalytic activity of Au/ZnO in different solvents are in the order of acetonitrile > THF > ethyl acetate > toluene. This could be possibly due to the unfavourable polarity or dielectric constant towards the intermediate as proposed by Biradar *et al*. (Biradar & Asefa, 2012), and possibly due to the larger solvent molecules that block the catalytic sites (Bhoware et al., 2006).

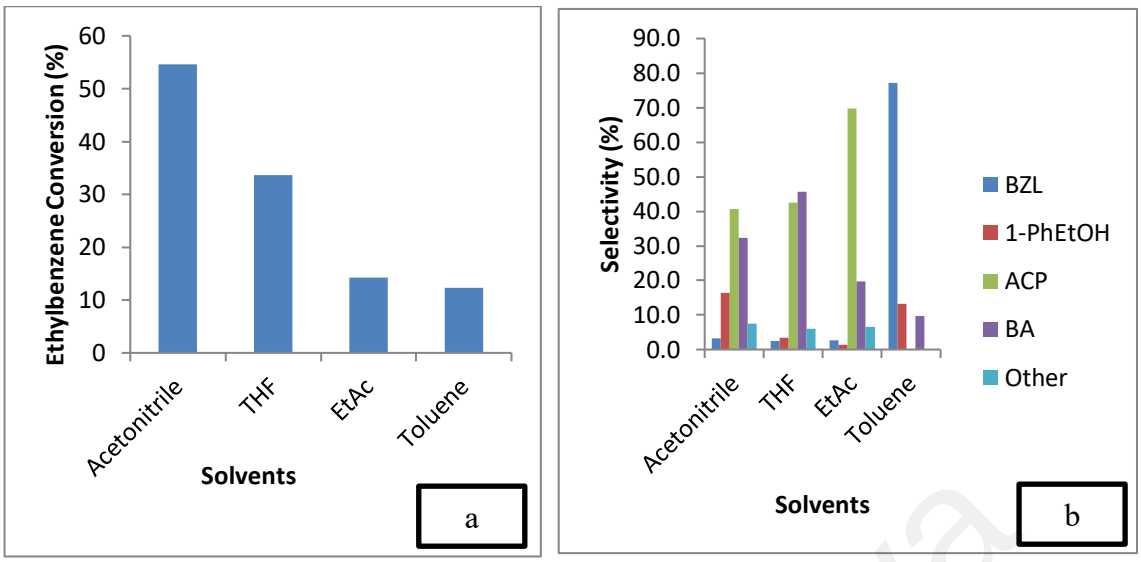

Figure 4.15: Effect of type of solvents to conversion of 0.2M ethylbenzene oxidation (a) and product selectivity (b) using 50 mg of 4wt% Au/ZnO at 100°C for 24 hours with 1mmol TBHP.

Generally, dipolar aprotic solvents such as THF gave better conversion compared to the non-polar solvents such as toluene and xylene, which have lower dipole moments and dielectric constants. Solvents with higher dielectric constants promote bond dissociation while solvents with lower dielectric constants neutralise the charged species by forming bonds (Carey & Sundberg, 2007). In addition, solvents with lower dipole moments and dielectric constants are hydrophobic and are detrimental to the conversion. Habibi *et al*. reported that the conversion reaction was inhibited in water, as the lone pair of electrons of the oxygen atom in the water molecules tends to block the active site of Au (Arshadi et al., 2012; Habibi et al., 2013).

Polar solvents are also favourable for the oxidation reaction such as the oxidation of cyclohexane, where the conversion increases with the solvent polarity. Jing *et al*. suggests that the π-bonds in the polar solvent reacts with the transition metal ions to form an intermediate which promotes the reaction (Jing et al., 2016). The type of solvent is relatively important since some solvents are co-oxidants, in addition produces another oxidizing agent which increases the rate of conversion (Andrade et al., 2005).

Acetonitrile is known to produce peroxy carboximidic acid, a powerful oxidizing agent, while THF promotes a radical oxidation process, thus these solvents gave higher conversion of ethylbenzene (Andrade et al., 2005). Hence, it is concluded that ethylbenzene conversion is optimized in acetonitrile as the solvent, regardless of the higher selectivity of other solvents.

4.2.5 Effect of Temperature

Figure 4.16 shows that the catalytic conversion is slightly increased with the increase of reaction temperature from 60 °C to 120 °C. The selectivity of ACP did not change significantly, however there is increased selectivity towards the by-products such as PE, BZL and Other at 120 °C. It seems that the reaction favours the release of more energy to break the C-C bond to form benzaldehyde. No benzaldehyde compound was observed at 60 ˚C since benzaldehyde was converted to benzoic acid. As the temperature increased, the oxidation of benzaldehyde to benzoic acid was reduced as the reaction was favored at low temperature (Arshadi & Ghiaci, 2011). Selectivity to other compounds at 120 ˚C are the highest compared to other temperatures possibly due to further oxidation of acetophenone and 1-phenylethanol (Mo et al., 2020).

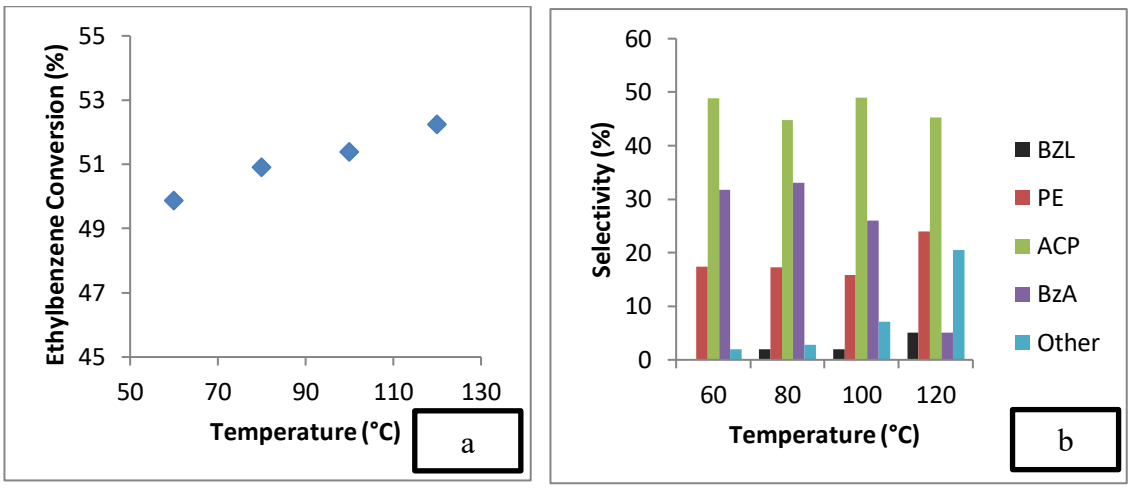

Figure 4.16: Effect of temperature on conversion of 0.2 M of ethylbenzene oxidation (a) and product selectivity (b) using 50 mg of 4 wt% Au/ZnO for 24 hours with 1 mmol TBHP.

4.2.6 Effect of Oxidant to EB Molar Ratio

Figure 4.17 shows the oxidation in the absence of TBHP (t-butyl hydroxyl peroxide) at 26.3% conversion of EB with high selectivity towards acetophenone at 84.8% and significant selectivity of PE at 15.2%. The reaction without TBHP was still taking place as oxygen gas from ambient pressure was involved in the reaction. It is noted from Figure 4.17 that no benzaldehyde was formed as the reaction without oxidation agent favors to the formation of acetophenone and 1-phenyethanol only due the limitation of oxygen from surrounding atmosphere. Therefore, no benzoic acid was formed as benzaldehyde was not presence. The increase in TBHP concentration gave a linear increase in the EB conversion as more TBHP radicals that supplies oxygen were available for the reaction. The selectivity of ACP and PE are almost constant from 2 to 4 mmol of TBHP. Addition of activated oxygen of co-coordinated TBHP into a C–H bond of the methylene group in EB produced PE. Subsequent abstraction of alcoholic OH hydrogen and the CH hydrogen of 1-phenylethanol would yield ACP or BZL. Both of the product can be further oxidize to benzoic acid (Kanjina & Trakarnpruk, 2011).

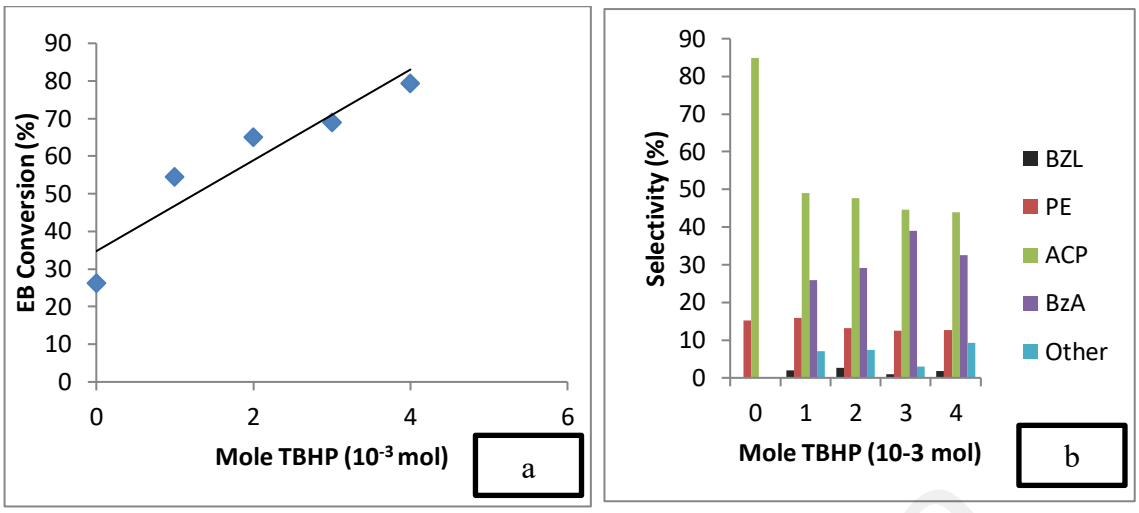

Figure 4.17: Effect of oxidant to substrate ratio for conversion of 0.2 M ethylbenzene oxidation (a) and product selectivity (b) using 50 mg of 4 wt% Au/ZnO at 100 °C for 24 hours.

Increasing of TBHP allow more secondary oxidation of other byproducts to occur which can be observed where ACP and PE remain almost stagnant while producing more benzoic acid from further oxidation of benzaldehyde which appear to be reduce as benzoic acid increase (Unnarkat et al., 2021). Small amount of benzaldehyde is observed with addition of TBHP because benzaldehyde went autoxidation to form benzoic acid with the presence of oxidation agent (Sankar et al., 2014). The catalyst also appear to be effective as at lower oxidant molar ratio (1:1) which is 1 mmol of TBHP able to achieve more than 50% conversion of EB while compare with other reported oxidation of EB which uses higher oxidant molar ratio such as (Chaudhary & Sharma, 2020; Unnarkat et al., 2021)

Other peroxide agent such as H_2O_2 (37% of H_2O_2) was used with no catalytic activity and selectivity were observed. This is possibly due to significant amount of water in H_2O_2 as H_2O deactivates the active sites of the catalyst (Arshadi et al., 2012). Since TBHP was the source of oxygen for the reaction, it is suggested that the conversion of ethylbenzene oxidation is proportional to the concentration of TBHP.

4.2.7 Effect of Catalyst Weight

To study the effect of catalyst weight on the oxidation reaction, TBHP and EB at 1:1 ratio was kept constant. As the catalyst was present at lower weight (10 mg), the conversion of EB increased to 46% as shown in Figure 4.18. The conversion gradually increased from 10 mg to 100 mg, suggesting that the amount becomes rate limiting at 10 mg onwards. As the catalyst amount exceeded 50 mg, the EB conversion slightly drop and remain unchanged probably due to the diffusion control factor (Ji et al., 2021). Selectivity for ACP increases as catalyst weight increases, which assuming presence of gold nanoparticles favor the reaction pathway toward ACP. It is also observed the highest selectivity of benzoic acid in Figure 4.18 shows at 63.0% in the reaction without catalyst. It is possibly due to present of TBHP as most benzaldehyde further oxidized to benzoic acid. However, the selectivity of benzoic acid is reduced from 10 mg to 40 mg catalyst possibly because most oxygen molecules from TBHP was adsorbed on the catalyst surface as depicted in the proposed reaction mechanism in Figure 4.12.

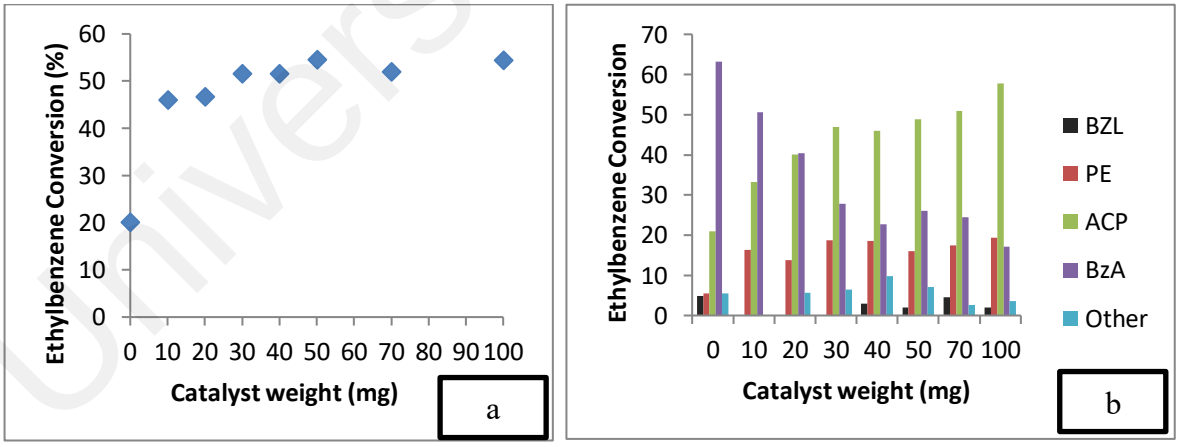

Figure 4.18: Effect of catalyst weight to conversion of 0.2 M ethylbenzene oxidation (a) and product selectivity (b) using 4wt% Au/ZnO at 100°C for 24 hours with 1 mmol of TBHP.

The surface area for the catalyst was increased as more catalyst was used in the reaction. Therefore, more TBHP adsorbed on the catalyst surface. The selectivity benzoic acid is constant around 20% from 40 mg to 100 mg due to lack of oxygen radical to oxidize benzaldehyde.

4.2.8 Effect of Au wt% Loading

The conversion of EB also depends on the amount of gold loading (wt%) in the catalyst, as shown in Figure 4.19. In the absence of the catalyst, the oxidation reaction shows 20.1% conversion of EB. ZnO shows slightly reduction in EB oxidation conversion as it was suggested ZnO adsorbed TBHP during reaction and significantly inhibited TBHP to react with ethylbenzene. Similar conversion for no catalyst was observed when 0.5 wt% Au on ZnO was used as catalyst with almost similar selectivity with ZnO catalyst. The product selectivity towards BzA was decreased while the selectivity towards ACP increased as more Au metal loading was used. The increasing gold loadings demonstrated higher conversion due to the presence of more Au nano particles that provide additional active sites for the catalytic activity. Therefore, the conversion of EB is proportional to the amount of gold loading, as more active sites are available.

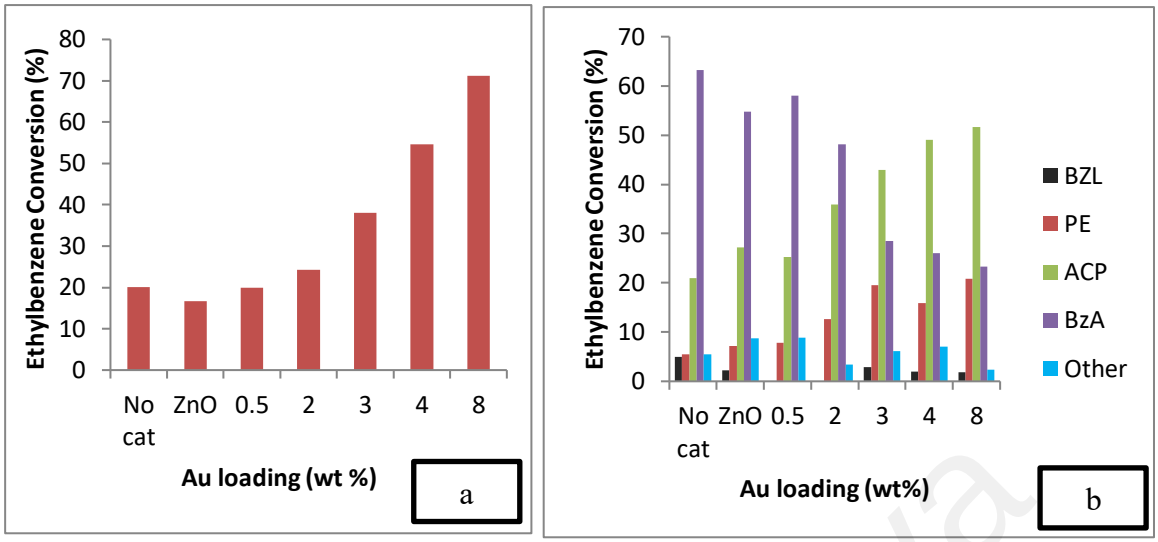

Figure 4.19: Effect of gold loading to conversion of 0.2 M ethylbenzene oxidation (a) and product selectivity (b) using 50mg of Au/ZnO at 100 °C for 24 hours with 1 mmol of TBHP.

However, higher metal nanoparticles loading also increases the tendency towards particle agglomeration and reduces the catalytic performance (Ji et al., 2021). Some studies reported that higher conversion could be achieved with larger size of gold nanoparticles between 6.9-8.4 nm (Biradar & Asefa, 2012; Haider et al., 2008). Surprisingly, Au/ZnO at high gold loading provide high conversion, further study may require in determining ~~at~~ the maximum gold loading efficiency of the catalyst. In term of selectivity, the benzoic acid selectivity using ZnO support is reduced at 54.7% due to adsorption of TBHP. The selectivity of benzoic acid is reduced significantly from 0.5 to 8 wt% Au as more TBHP was adsorbed on the active sites of Au metal catalyst. The increasing Au loading had increased the active sites of the catalyst that lead to high adsorption of oxygen radicals from TBHP. Therefore, less oxygen available for the oxidation of benzaldehyde to benzoic acid.

4.2.9 Effect of Volume

Volume of feed also played an important role in the catalyst performance, as shown in Figure 4.20 as ACN used is higher when higher feed volume was used. Six different volumes, 3, 5, 7, 10, 13 and 15 mL were tested and the conversion percentages were determined after 24 h of reaction. As observed in Figure 4.20, the increase in substrate volume which corresponds to the increase in solvent volume led to a significant decrease in the catalytic conversion with time, similar to the report by Titinchi *et al*. (Titinchi et al., 2015). The reaction performed at higher volume shows lower catalytic activity. The conversion of ethyl benzene and selectivity of acetophenone is disproportional with the feed volume. This could be due to the inhibition of active sites by the solvent molecules, thus creating a diffusion competition between the solvent and the substrate (Bhoware et al., 2006). It is demonstrated that larger solvent volume contributes to lower conversion, as the higher solvent ratio suppresses the analyte, thereby lowering the reaction rates (Titinchi et al., 2015). This finding is also supported by the results of Arshadi *et al*., where the catalytic activity was higher in solvent free condition than in the presence of ACN (Arshadi & Ghiaci, 2011). However, due to the absence of a highly efficient reflux system, a detailed analysis of the solvent-free method was not possible, as the products were completely dried out before it could be analysed using GC. Due to the same reason, almost 3 mL of volume will be lost after reaction, thus making 5 mL is the optimum volume as the volume recovered from a 3 mL volume substrate was inconsistent and sometimes insufficient for further testing using GC. It is also noted in Figure 4.20 that the benzoic acid selectivity is increased with the increasing of acetonitrile solvent volume. This trend was expected as acetonitrile is also an oxidizing agent that that can oxidize benzaldehyde to benzoic acid during reaction. Therefore, feed volume around 5 mL was sufficient to ensure

acceptable ethyl benzene conversion with high acetophenone and minimum benzoic acid selectivity's.

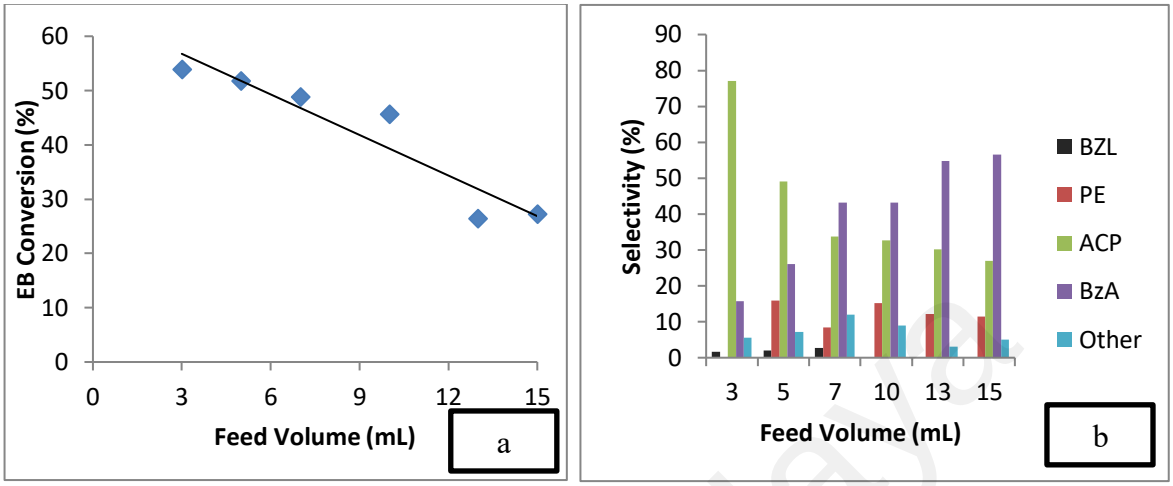

Figure 4.20: Effect of total feed volume to conversion of ethylbenzene oxidation 0.2 M (a) and product selectivity (b) using 50 mg of 4wt% Au/ZnO at 100°C for 24 hours.

4.3 Catalytic Studies on Benzyl alcohol Oxidation

Another substrate of interest studied in this work was benzyl alcohol. Benzyl alcohol (BA) is much easier to oxidize due to the presence of free electro-valances of oxygen. Benzyl alcohol oxidation was performed under reflux in which reaction time at 8 hours, temperature 80 °C, ambient pressure using 30 mg of 4 wt% Au/ZnO catalyst, TBHP as oxidation agent with acetonitrile as solvent.

The benzyl alcohol oxidation reaction without catalyst and with catalyst was tested using standard process condition (8 hours reaction time and 80 °C reaction temperature). In the catalyst absence, benzyl alcohol was oxidized at 7 % conversion. This reaction was observed possibly due to the significant reaction between the substrate, benzyl alcohol and the oxidising agent, TBHP itself. ZnO support is active as catalyst as it act as co-catalyst for oxidation reaction when ZnO is calcined (Amigues &

Teichner, 1966). The reaction showed 9.0% conversion when ZnO was tested in benzy alcohol oxidation reaction. With the presence of 4wt% of gold on ZnO it significantly increased the benzyl alcohol conversion at 60% conversion at 80 °C reaction temperature.

4.3.1 Effect of the Feed Concentration and Temperature

Figure 4.21 shows the reaction conversion at 0.02 M and 0.2 M of benzyl alcohol at different reaction temperature. The concentration of 0.02 M and 0.2 M of benzyl alcohol at 25 ºC (room temperature) shows conversion at 9 % and 2 % respectively at low reaction temperature.

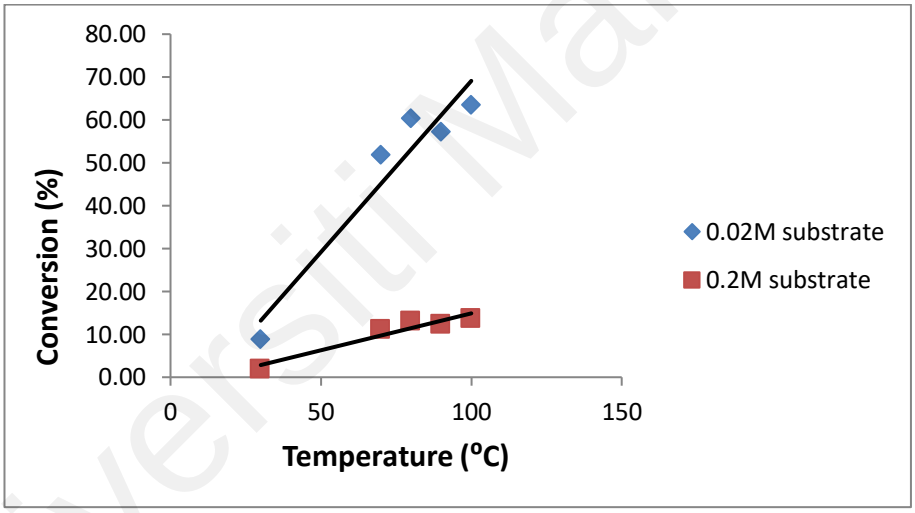

Figure 4.21: Effect of substrate concentration and the reaction temperature.

As the reaction temperature is increased to 70 °C, the conversion of benzyl alcohol at 0.02 M shoot up to almost 52 % while 0.2 M benzyl alcohol is slightly increased to 11.0 %. It was suggested the conversion was increased 5 times higher in 10 times less diluted benzyl alcohol substrate because it was more efficient for substrate to adsorbed on Au active sites. Inversely, the substrate is less efficient to adsorbed on Au active sites because the catalyst was not efficient to facilitate accessibility to many reactant molecules at high concentration (Herron & Corbin, 1995). The conversion remains constant for 0.2 M benzyl alcohol from 80 ˚C to 100 ˚C due to problems for the

substrate to access Au active sites on catalyst surface. This suggestion is supported by JamJam and co-worker as Au sites responsible for the high selectivity of benzaldehyde (JamJam et al., 2019).

The catalytic activity of benzyl alcohol for 0.02 M increases at 60.3 % as the temperature reaches 80 °C. However, the conversion is slightly dropped to 57.2% at 90 °C due to presence of benzoic acid as side product. The benzoic acid is presence usually due to further oxidation of the main product, benzaldehyde. In this research study, selectivity towards benzaldehyde is the focus thus reaction at higher temperature than 80 ^{0}C is not preferable even though the conversion of benzyl alcohol is high. From the data, it seems that benzaldehyde appear to be stable at high selectivity toward benzaldehyde at temperature lower than 90 °C. Therefore, it is proposed the substrate concentration at 0.02 M was better than substrate concentration at 0.2 M when catalyst amount of 30 mg (4wt% Au/ZnO) was used with reaction temperature at 80 °C in 8 hours reaction time.

4.4 Catalyst Stability & Recyclability

The Au/ZnO catalyst was stable for 8 months in a refrigerator at -5 °C with only a slight reduce of particle size which is less than 1 nm. Figure 4.22 shows the gold particle size of 3.04 ± 0.88 nm after storage for 8 months compared to a freshly synthesized catalyst size of 2.31 ± 0.42 nm (Figure 4.9). The ethylbenzene oxidation also shows decrease at about 2% in conversion using 8 months old Au/ZnO catalyst shown in Table 4.2.

It can be concluded that both uncalcined gold and calcined gold were unstable at ambient air, as the uncalcined gold was reduced/degraded upon sintering of the gold particles (Zanella & Louis, 2005). Thus, it is recommended that the catalyst gold nanoparticles should be stored in the dark under vacuum or nitrogen atmosphere at low temperatures.

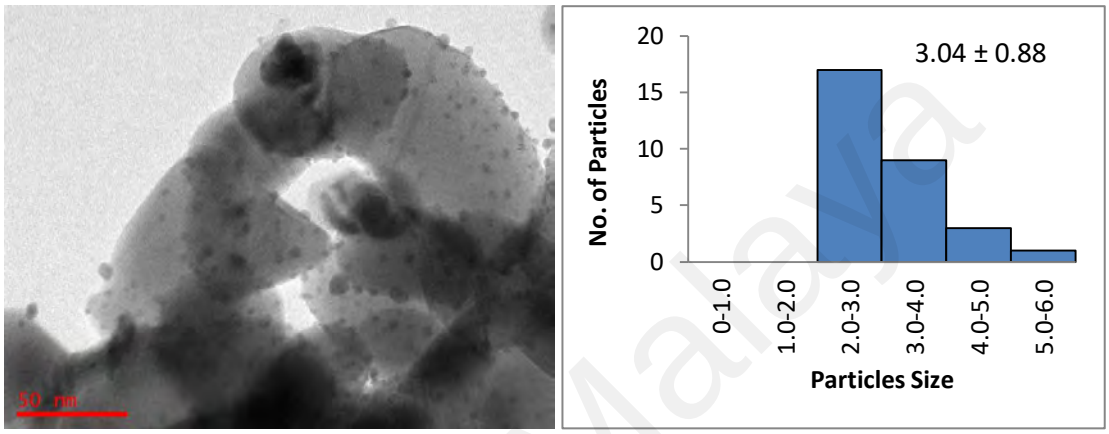

Figure 4.22: TEM image at 50 nm scale images with 200kV of calcined gold 2 wt% on zinc oxide stored up to 8 months and particle distribution graph.

A recycling study for the Au/ZnO catalyst (4 wt%) in ethylbenzene oxidation was performed under the optimized reaction conditions. Table 4.2 shows that the ethylbenzene conversion reduced half at to 23.6% in the second cycle reaction. The selectivity towards acetophenone, 1-phenylethanol and benzaldehyde decreases, while a higher tendency towards benzoic acid was observed, as the benzaldehyde was further oxidized to benzoic acid when exposed to air (Oliveira et al., 2017). The decrease in ethylbenzene conversion and product selectivity could be due to the leaching phenomenon, where the leached metal deposited out from the support reduced during ethyl benzene oxidation reaction. As shown in table 4.1 where a decrease of 0.6 Au wt % from spent catalyst (after reaction).

CHAPTER 5: CONCLUSION

5.1 Conclusion

To conclude, gold nanoparticles were synthesized on zinc oxide supports and proved to be an efficient catalyst for the oxidation of ethylbenzene and benzyl alcohol. The average size of gold nanoparticles were ~3 nm, supported on ZnO with maximum gold loading of 8 wt% were successfully prepared. Based on the characterization study it was observed that calcination played a vital role in activating the gold nanoparticles and relatively increased the degree of crystallinity of ZnO in improving the catalytic activity for ethylbenzene and benzylalcohol oxidations. ATR-FTIR also shows no trace of urea in the synthesized catalyst which provides better catalyst activation without any contamination in the catalyst synthesis and catalyst washing. TEM images show that calcination step insignificantly changed the particle size of AuNPs with 1nm difference between uncalcined and calcined catalysts. This result was further confirmed by XRD analysis that showed no Au diffraction peaks due to small sized gold particles (<5 nm) for both calcined and uncalcined catalysts. In terms of elemental analysis by XRF, it was found that the prepared catalysts were slightly reduced in terms of compound element percentage as compared to the intended 4 wt% Au/ZnO possibly because gold particles were not fully deposited on ZnO support due to the washing step and poor interaction with support material which caused the AuNPs to leached out from ZnO. From BET results it was found that the deposition of gold on ZnO support increases the total surface area (m^2/g), while the pore size slightly decreases as AuNPs was deposited in the pores. It is assumed that the size of AuNPs is very small which covers the surface area and fills the pore volume of the ZnO as voids in ZnO mesopores were occupied by

the Au. This suggests an enhancement of the texture properties of mesoporous ZnO after Au deposition.

On the catalytic activity it is shown that the prepared nano catalysts are very promising in ethylbenzene and benzyl alcohol oxidations. A significant conversion was observed from ethylbenzene catalysis producing acetophenone as major product while 1- phenylethanol, benzaldehyde, benzoic acid and others as by products. A series of reaction variable was performed towards ethylbenzene oxidation including type of solvent, feed volume, catalyst weight, gold loading (wt%), reaction time and reaction temperature. It was found the optimized reaction using acetonitrile as solvent, 5 mL of feed volume, catalyst weight of 50 mg, higher gold loading (8 wt%), and 1:1 oxidant molar ratio. Overall, the catalyst performance has been found very effective in the EB oxidation reaction with minimum amount of TBHP, solvent used and catalyst weight.

On top of that, the catalyst also showed high catalytic activity in benzyl alcohol oxidation with 100% selectively of benzaldehyde with conversion 60% in 8 hours reaction. No formation of by-products was observed when the reaction was performed at ambient pressure with benzyl alcohol concentration at 0.02 M, using 30 mg of catalyst in acetonitrile solvent at temperature below than 90 ˚C. However, the reaction would produce other side products such as, benzoic acid due to further oxidation of benzaldehyde.

The 4 wt% Au/ZnO catalyst was found to be active for 8 months in a freezer at -5 ˚C in absence of light exposure. This catalyst showed small particle size increased and similar catalytic activity compared to freshly calcined 4 wt% Au/ZnO.

5.2 Future Work

Several future directions related to this research were identified, and listed as follows: -

- To identify and study the other compound to complete the proposed reaction mechanism of ethyl benzene oxidation reaction.
- Encapsulate the gold nanoparticles on the metal oxide in order to increase the interaction of AuNPs on ZnO thus preventing metal leaching during reaction.
- A comprehensive mechanism study on ethylbenzene and benzylalcohol reaction.

REFERENCES

Adnan, R. H., Andersson, G. G., Polson, M. I. J., Metha, G. F., & Golovko, V. B. (2015). Factors influencing the catalytic oxidation of benzyl alcohol using supported phosphine-capped gold nanoparticles. *Catalysis Science & Technology*, *5*(2), 1323-1333.

Aguilar-Tapia, A., Delannoy, L., Louis, C., Han, C. W., Ortalan, V., & Zanella, R. (2016). Selective hydrogenation of 1,3-butadiene over bimetallic Au-Ni/TiO2 catalysts prepared by deposition-precipitation with urea. *Journal of Catalysis*, *344*, 515-523.

Akhtar, M. J., Ahamed, M., Kumar, S., Khan, M. M., Ahmad, J., & Alrokayan, S. A. (2012). Zinc oxide nanoparticles selectively induce apoptosis in human cancer cells through reactive oxygen species. *International Journal of Nanomedicine*, *7*, 845-857.

Al-Hada, N. M., Saion, E. B., Shaari, A. H., Kamarudin, M. A., Flaifel, M. H., Ahmad, S. H., & Gene, S. A. (2014). A facile thermal-treatment route to synthesize ZnO nanosheets and effect of calcination temperature. *PLOS ONE*, *9*(8), Article ID 103134.

Alabbad, S., Adil, S. F., Assal, M. E., Khan, M., Alwarthan, A., & Siddiqui, M. R. H. (2014). Gold & silver nanoparticles supported on manganese oxide: Synthesis, characterization and catalytic studies for selective oxidation of benzyl alcohol. *Arabian Journal of Chemistry*, *7*(6), 1192-1198.

Ali, M. E., Hashim, U., Mustafa, S., Che Man, Y. B., & Islam, K. N. (2012). Gold Nanoparticle Sensor for the Visual Detection of Pork Adulteration in Meatball Formulation. *Journal of Nanomaterials*, *2012*, 7, Article ID 103607.

Ali, M. E., Rahman, M. M., & Hamid, S. B. A. (2014). Nanoclustered Gold: A Promising Green Catalysts for the Oxidation of Alkyl Substituted Benzenes. *Advanced Materials Research*, *925*, 38-42.

Amigues, P., & Teichner, S. J. (1966). Mechanism of the catalytic oxidation of carbon monoxide on zinc oxide. *Discussions of the Faraday Society*, *41*(0), 362-379.

Andrade, Z., Carlos, K., & Alves, L. M. (2005). Environmentally benign solvents in organic synthesis: Current topics. *Current Organic Chemistry*, *9*(2), 195-218.

Armor, J. N. (2001). New catalytic technology commercialized in the USA during the 1990s. *Applied Catalysis A: General*, *222*(1), 407-426.

Arshadi, M., & Ghiaci, M. (2011). Highly efficient solvent free oxidation of ethylbenzene using some recyclable catalysts: The role of linker in competency of manganese nanocatalysts. *Applied Catalysis A: General*, *399*(1), 75-86.

Arshadi, M., Ghiaci, M., Rahmanian, A., Ghaziaskar, H., & Gil, A. (2012). Oxidation of ethylbenzene to acetophenone by a Mn catalyst supported on a modified nanosized SiO2/Al2O3 mixed-oxide in supercritical carbon dioxide. *Applied Catalysis B: Environmental*, *119-120*, 81-90.

Bahar, N., & Ekinci, D. (2020). Hollow porous gold nanoparticle/reduced graphene oxide composite films for electrochemical supercapacitor applications. *Electrochimica Acta*, *337*, Article ID 135844.

Bhoware, S. S., Shylesh, S., Kamble, K. R., & Singh, A. P. (2006). Cobalt-containing hexagonal mesoporous molecular sieves (Co-HMS): Synthesis, characterization and catalytic activity in the oxidation reaction of ethylbenzene. *Journal of Molecular Catalysis A: Chemical*, *255*(1), 123-130.

Biradar, A. V., & Asefa, T. (2012). Nanosized gold-catalyzed selective oxidation of alkyl-substituted benzenes and n-alkanes. *Applied Catalysis A: General*, *435-436*, 19-26.

Bond, G. (2008). The early history of catalysis by gold. *Gold Bulletin*, *41*(3), 235-241.

Bond, G., Louis, C., & Thompson, D. (2006). *Catalytic Science Series, Vol. 6, Catalysis by Gold*. London, UK: Imperial College Press.

Bond, G. C., Sermon, P. A., Webb, G., Buchanan, D. A., & Wells, P. B. (1973). Hydrogenation over supported gold catalysts. *Journal of the Chemical Society, Chemical Communications, 13*, 444-445.

Campbell, I. M. (1988). *Catalysis at Surfaces.* Netherlands: Springer.

Carabineiro, S. A. C., Chen, X., Martynyuk, O., Bogdanchikova, N., Avalos-Borja, M., Pestryakov, A., . . . Figueiredo, J. L. (2015). Gold supported on metal oxides for volatile organic compounds total oxidation. *Catalysis Today*, *244*, 103-114.

Carabineiro, S. A. C., & Thompson, D. T. (2007). Catalytic Applications for Gold Nanotechnology. In U. Heiz & U. Landman (Eds.), *Nanocatalysis* (pp. 377-489). Heidelberg, Berlin: Springer.

Carey, F. A., & Sundberg, R. J. (2007). *Advanced Organic Chemistry: Part A - Structure and Mechanisms*. Boston, MA: Springer Science & Business Media.

Carlsson, J.-O., & Martin, P. M. (2010). Chapter 7 - Chemical Vapor Deposition. In P. M. Martin (Ed.), *Handbook of Deposition Technologies for Films and Coatings (Third Edition)* (pp. 314-363). Norwich, NY: William Andrew Publishing.

Chandra, P., Singh, J., Singh, A., Srivastava, A., Goyal, R. N., & Shim, Y. B. (2013). Gold Nanoparticles and Nanocomposites in Clinical Diagnostics Using Electrochemical Methods. *Journal of Nanoparticles*, *2013*, 12, Article ID 535901.

Chatterjee, A. K. (2001). X-Ray Diffraction. In V. S. Ramachandran & J. J. Beaudoin (Eds.), *Handbook of Analytical Techniques in Concrete Science and Technology* (pp. 275-332). Norwich, NY:William Andrew Publishing.

Chaudhary, V., & Sharma, S. (2021). Study of ethylbenzene oxidation over polymer-silica hybrid supported Co (II) and Cu (II) complexes. *Catalysis Today, 375*, 601-613.

Chen, Y.-H., Mou, C.-Y., & Wan, B.-Z. (2017). Ultrasmall gold nanoparticles confined in zeolite Y: Preparation and activity in CO oxidation. *Applied Catalysis B: Environmental*, *218*, 506-514.

Chen, Y., Zheng, H., Guo, Z., Zhou, C., Wang, C., Borgna, A., & Yang, Y. (2011). Pd catalysts supported on MnCeOx mixed oxides and their catalytic application in solvent-free aerobic oxidation of benzyl alcohol: Support composition and structure sensitivity. *Journal of Catalysis*, *283*(1), 34-44.

Costa, V. V., Estrada, M., Demidova, Y., Prosvirin, I., Kriventsov, V., Cotta, R. F., . . . Gusevskaya, E. V. (2012). Gold nanoparticles supported on magnesium oxide as catalysts for the aerobic oxidation of alcohols under alkali-free conditions. *Journal of Catalysis*, *292*, 148-156.

Cushing, B. L., Kolesnichenko, V. L., & O'Connor, C. J. (2004). Recent Advances in the Liquid-Phase Syntheses of Inorganic Nanoparticles. *Chemical Reviews*, *104*(9), 3893-3946.

Dai, X., Li, X., Tang, S., Peng, X., Zheng, X., & Jiang, O. (2021). Efficient aerobic oxidation of ethylbenzene accelerated by cu species in hydrotalcite. *Catalysis Communications*, *149*, Article ID 106184.

Dapurkar, S. E., Shervani, Z., Yokoyama, T., Ikushima, Y., & Kawanami, H. (2009). Supported Gold Nanoparticles Catalysts for Solvent-free Selective Oxidation of Benzylic Compounds into Ketones at 1 atm O2. *Catalysis Letters*, *130*(1-2), 42-47.

Daruich De Souza, C., Ribeiro Nogueira, B., & Rostelato, M. E. C. M. (2019). Review of the methodologies used in the synthesis gold nanoparticles by chemical reduction. *Journal of Alloys and Compounds*, *798*, 714-740.

Dehghan Banadaki, A., & Kajbafvala, A. (2014). Recent Advances in Facile Synthesis of Bimetallic Nanostructures: An Overview. *Journal of Nanomaterials*, *2014*, 28, Article ID 985948.

Devika, S., Palanichamy, M., & Murugesan, V. (2011). Selective oxidation of ethylbenzene over CeAlPO-5. *Applied Catalysis A: General*, *407*, 76-84.

Dimitratos, N., Villa, A., Bianchi, C. L., Prati, L., & Makkee, M. (2006). Gold on titania: Effect of preparation method in the liquid phase oxidation. *Applied Catalysis A: General*, *311*, 185-192.

Dobrosz, I., Jiratova, K., Pitchon, V., & Rynkowski, J. M. (2005). Effect of the preparation of supported gold particles on the catalytic activity in CO oxidation reaction. *Journal of Molecular Catalysis A: Chemical*, *234*(1), 187-197.

Donnet, J.-B., & Custodero, E. (2013). Chapter 8 - Reinforcement of Elastomers by Particulate Fillers. In J. E. Mark, B. Erman, & C. M. Roland (Eds.), *The Science and Technology of Rubber (Fourth Edition)* (pp. 383-416). Cambridge, MA: Academic Press.

Du, M., Sun, D., Yang, H., Huang, J., Jing, X., Odoom-Wubah, T., . . . Li, Q. (2014). Influence of Au particle size on Au/TiO2 catalysts for CO oxidation. *The Journal of Physical Chemistry C*, *118*(33), 19150-19157.

Edwards, P. P., & Thomas, J. M. (2007). Gold in a Metallic Divided State—From Faraday to Present-Day Nanoscience. *Angewandte Chemie International Edition*, *46*(29), 5480-5486.

Engel, T., & Ertl, G. (1979). Elementary Steps in the Catalytic Oxidation of Carbon Monoxide on Platinum Metals. In D. D. Eley, H. Pines, & P. B. Weez (Eds.), *Advances in Catalysis* (Vol. 28, pp. 1-78). Cambridge, MA: Academic Press.

Engineers Daily. (2014). *Qualitative Analysis with X-Ray Diffraction (XRD)*. Retrieved on 13 August 2021 from https://www.engineersdaily.com/2014/03/qualitative-analysis-with-x-ray-diffraction-xrd.html

Fackler, J. P. (2007). Book Review of Catalysis by Gold. *Journal of the American Chemical Society*, *129*(13), 4107-4107.

Fang, X., Sharma, M., Stennett, C., & Gill, P. P. (2017). Optical sensitisation of energetic crystals with gold nanoparticles for laser ignition. *Combustion and Flame*, *183*, 15-21.

Fujita, T., Horikawa, M., Takei, T., Murayama, T., & Haruta, M. (2016). Correlation between catalytic activity of supported gold catalysts for carbon monoxide oxidation and metal–oxygen binding energy of the support metal oxides. *Chinese Journal of Catalysis*, *37*(10), 1651-1655.

Furusaki, S. (2001). *The Expanding World of Chemical Engineering* (2nd ed.). Oxfordshire, UK: Taylor & Francis Group.

Ganesh Kumar, C., Pombala, S., Poornachandra, Y., & Vinod Agarwal, S. (2016). Chapter 4 - Synthesis, characterization, and applications of nanobiomaterials for antimicrobial therapy. In A. M. Grumezescu (Ed.), *Nanobiomaterials in Antimicrobial Therapy* (pp. 103-152). Norwich, NY: William Andrew Publishing.

Gangopadhyay, D., Singh, D. S., Sharma, P., Mishra, H., V K, U., Singh, B., & Singh, R. (2016). Spectroscopic and structural study of the newly synthesized heteroligand complex of copper with creatinine and urea. *Spectrochimica Acta Part A: Molecular and Biomolecular Spectroscopy, 154,* 201-206.

Ghadamgahi, S., Williamson, B. E., & Golovko, V. B. (2016). Activity of Catalysts Derived from Au101 Immobilized on Activated Carbon. *Catalysis Letters*, *146*(6), 1027-1032.

Habibi, D., Faraji, A. R., Arshadi, M., & Fierro, J. L. G. (2013). Characterization and catalytic activity of a novel Fe nano-catalyst as efficient heterogeneous catalyst for selective oxidation of ethylbenzene, cyclohexene, and benzylalcohol. *Journal of Molecular Catalysis A: Chemical*, *372*, 90-99.

Habibi, D., Faraji, A. R., Arshadi, M., Veisi, H., & Gil, A. (2014). Manganese nanocatalyst and N-hydroxyphthalimide as an efficient catalytic system for selective oxidation of ethylbenzene, cyclohexene and oximes under aerobic condition. *Journal of Molecular Catalysis A: Chemical*, *382*, 41-54.

Haider, P., Kimmerle, B., Krumeich, F., Kleist, W., Grunwaldt, J.-D., & Baiker, A. (2008). Gold-Catalyzed Aerobic Oxidation of Benzyl Alcohol: Effect of Gold Particle Size on Activity and Selectivity in Different Solvents. *Catalysis Letters*, *125*(3), 169-176.

Haruta, M. (1997). Size- and support-dependency in the catalysis of gold. *Catalysis Today*, *36*(1), 153-166.

Haruta, M. (2004). Gold as a novel catalyst in the 21st century: Preparation, working mechanism and applications. *Gold Bulletin*, *37*(1), 27-36.

Haruta, M. (2011). Spiers Memorial Lecture Role of perimeter interfaces in catalysis by gold nanoparticles. *Faraday Discussions*, *152*(0), 11-32.

Haruta, M. (2014). Chance and necessity: My encounter with gold catalysts. *Angewandte Chemie International Edition in English*, *53*(1), 52-56.

Haruta, M., Kobayashi, T., Sano, H., & Yamada, N. (1987). Novel gold catalysts for the oxidation of carbon monoxide at a temperature far below 0°C. *Chemistry Letters*, *16*(2), 405-408.

Haruta, M., Ueda, A., Tsubota, S., & Torres Sanchez, R. M. (1996). Low-temperature catalytic combustion of methanol and its decomposed derivatives over supported gold catalysts. *Catalysis Today*, *29*(1), 443-447.

Herron, N., & Corbin, D. R. (1995). *Inclusion Chemistry with Zeolites: Nanoscale Materials by Design* (Vol. 6). Dordrecht, Netherlands: Springer.

Hind, A. R., Bhargava, S. K., & McKinnon, A. (2001). At the solid/liquid interface: FTIR/ATR — the tool of choice. *Advances in Colloid and Interface Science*, *93*(1), 91-114.

Hong, Y., Jing, X., Huang, J., Sun, D., Odoom-Wubah, T., Yang, F., . . . Li, Q. (2014). Biosynthesized Bimetallic Au–Pd Nanoparticles Supported on TiO2 for Solvent-Free Oxidation of Benzyl Alcohol. *ACS Sustainable Chemistry & Engineering*, *2*(7), 1752-1759.

Hoyos-Palacio, L. M., Cuesta Castro, D. P., Ortiz-Trujillo, I. C., Botero Palacio, L. E., Galeano Upegui, B. J., Escobar Mora, N. J., & Carlos Cornelio, J. A. (2019). Compounds of carbon nanotubes decorated with silver nanoparticles via in-situ by chemical vapor deposition (CVD). *Journal of Materials Research and Technology*, *8*(6), 5893-5898.

Hua, J. (2021). Synthesis and characterization of gold nanoparticles (AuNPs) and ZnO decorated zirconia as a potential adsorbent for enhanced arsenic removal from aqueous solution. *Journal of Molecular Structure*, *1228*, Article ID 129482.

Hulla, J., Sahu, S., & Hayes, A. (2015). Nanotechnology:History and future. *Human & Experimental Toxicology*, *34*(12), 1318-1321.

Hussain, C. M., & Keçili, R. (2020). Chapter 7 - Separation techniques for environmental analysis. In C. M. Hussain & R. Keçili (Eds.), *Modern Environmental Analysis Techniques for Pollutants* (pp. 163-198). Amsterdam, Netherland: Elsevier.

Hutchings, G. J. (1985). Vapor phase hydrochlorination of acetylene: Correlation of catalytic activity of supported metal chloride catalysts. *Journal of Catalysis*, *96*(1), 292-295.

Ismail, A. A., Harraz, F. A., Faisal, M., El-Toni, A. M., Al-Hajry, A., & Al-Assiri, M. (2016). A sensitive and selective amperometric hydrazine sensor based on mesoporous Au/ZnO nanocomposites. *Materials & Design*, *109*, 530-538.

Jafari Eskandari, M., Shafyei, A., & Karimzadeh, F. (2020). One-step fabrication of Au@Al2O3 core-shell nanoparticles by continuous-wave fiber laser ablation of thin gold layer on aluminum surface: Structural and optical properties. *Optics & Laser Technology*, *126*, Article ID 106066.

Jain, A., Zhao, X., Kjergaard, S., & Stagg-Williams, S. M. (2005). Effect of aging time and calcination on the preferential oxidation of CO over Au supported on doped ceria. *Catalysis Letters*, *104*(3), 191-197.

JamJam, N. M., Taufiq Yap, Y. H., Muhamad, E. N., Izham Saiman, M., & Saleh, T. A. (2019). Free solvent oxidation of molecular benzyl alcohol by newly synthesized AuPd/titania catalysts. *Inorganic Chemistry Communications*, *107*, Article ID 107471.

Jamkhande, P. G., Ghule, N. W., Bamer, A. H., & Kalaskar, M. G. (2019). Metal nanoparticles synthesis: An overview on methods of preparation, advantages and disadvantages, and applications. *Journal of Drug Delivery Science and Technology*, *53*, Article ID 101174.

Jaroniec, M., Kruk, M., & Sayari, A. (1998). Adsorption methods for characterization of surface and structural properties of mesoporous molecular sieves. In L. Bonneviot, F. Béland, C. Danumah, S. Giasson, & S. Kaliaguine (Eds.), *Studies in Surface Science and Catalysis* (Vol. 117, pp. 325-332). Amsterdam, Netherlands: Elsevier.

Jawale, D. V., Gravel, E., Geertsen, V., Li, H., Shah, N., Kumar, R., . . . Doris, E. (2014). Size effect of gold nanoparticles supported on carbon nanotube as catalysts in selected organic reactions. *Tetrahedron*, *70*(36), 6140-6145.

Ji, D., Xi, N., Li, G., Dong, P., Li, H., Li, H., . . . Zhao, Y. (2021). Hydrotalcite-based CoxNiyAl1Ox mixed oxide as a highly efficient catalyst for selective ethylbenzene oxidation. *Molecular Catalysis*, *508*, Article ID 111579.

Jiménez-Pérez, Z. E., Singh, P., Kim, Y.-J., Mathiyalagan, R., Kim, D.-H., Lee, M. H., & Yang, D. C. (2017). Applications of Panax ginseng leaves-mediated gold nanoparticles in cosmetics relation to antioxidant, moisture retention, and whitening effect on B16BL6 cells. *Journal of Ginseng Research 42*(3), 327-333.

Jing, B.-q., Li, J.-f., & Qin, Z.-f. (2016). Selective oxidation of cyclohexane over Co-APO-5: Effects of solvent and modification method on the catalytic performance. *Journal of Fuel Chemistry and Technology*, *44*(10), 1249-1258.

Joshi, M., Bhattacharyya, A., & Ali, S. W. (2008). Characterization techniques for nanotechnology applications in textiles. *Indian Journal of Fibre and Textile Research*, *33*(3), 304-317.

Kaboudin, B., Saghatchi, F., & Kazemi, F. (2019). Synthesis of decorated carbon nanotubes with Fe3O4 and Au nanoparticles and their application in catalytic oxidation of alcohols in water. *Journal of Organometallic Chemistry*, *882*, 64-69.

Kamat, P. V. (2002). Photophysical, Photochemical and Photocatalytic Aspects of Metal Nanoparticles. *The Journal of Physical Chemistry B*, *106*(32), 7729-7744.

Kanjina, W., & Trakarnpruk, W. (2011). Mixed metal oxide catalysts for the selective oxidation of ethylbenzene to acetophenone. *Chinese Chemical Letters*, *22*, 401-404.

Khan, S., Runguo, W., Tahir, K., Jichuan, Z., & Zhang, L. (2017). Catalytic reduction of 4-nitrophenol and photo inhibition of Pseudomonas aeruginosa using gold nanoparticles as photocatalyst. *Journal of Photochemistry and Photobiology B: Biology*, *170*, 181-187.

Khoudiakov, M., Gupta, M. C., & Deevi, S. (2005). Au/Fe2O3 nanocatalysts for CO oxidation: A comparative study of deposition–precipitation and coprecipitation techniques. *Applied Catalysis A: General*, *291*(1), 151-161.

Kieboom, A.P. (1999). Chapter 1-History of catalysis. In J. A. Moulijn, P. W. N. M. van Leeuwen, & R. A. van Santen (Eds.), *Studies in Surface Science and Catalysis* (Vol. 123, pp. 3-28). Amsterdam, Netherland: Elsevier Science.

Kołodziejczak-Radzimska, A., Markiewicz, E., & Jesionowski, T. (2012). *Structural Characterisation of ZnO Particles Obtained by the Emulsion Precipitation Method*, *2012*, Article ID 656353.

Kramar, U. (2017). X-Ray Fluorescence Spectrometers. In J. C. Lindon, G. E. Tranter, & D. W. Koppenaal (Eds.), *Encyclopedia of Spectroscopy and Spectrometry (Third Edition)* (pp. 695-706). Cambridge, MA: Academic Press.

Li, D., & Liu, S. (2019). Chapter 11 - Groundwater Quality Detection. In D. Li & S. Liu (Eds.), *Water Quality Monitoring and Management* (pp. 269-302). Cambridge, MA: Academic Press.

Li, Y., Huang, J., Hu, X., Lam, F. L.-Y., Wang, W., & Luque, R. (2016). Heterogeneous Pd catalyst for mild solvent-free oxidation of benzyl alcohol. *Journal of Molecular Catalysis A: Chemical*, *425*, 61-67.

LibreTexts. (2020). *Instrumental Analysis - Spectrometer: ATR-FTIR*. Retrieved on 13 August 2021 from https://chem.libretexts.org/Bookshelves/Analytical_Chemistry/Supplemental_Modules_(Analytical_Chemistry)/Instrumental_Analysis/Spectrometer/ATR-FTIR

Lin, J.-N., & Wan, B.-Z. (2003). Effects of preparation conditions on gold/Y-type zeolite for CO oxidation. *Applied Catalysis B: Environmental*, *41*(1), 83-95.

Lindström, B., & Pettersson, L. J. (2003). A Brief History of Catalysis. *CATTECH*, *7*(4), 130-138.

Liu, C.-H., Lin, C.-Y., Chen, J.-L., Lu, K.-T., Lee, J.-F., & Chen, J.-M. (2017). SBA-15-supported Pd catalysts: The effect of pretreatment conditions on particle size and its application to benzyl alcohol oxidation. *Journal of Catalysis*, *350*, 21-29.

Liu, H. (2011). *Ammonia Synthesis Catalysts: Innovation and Practice.* Shanghai, China: Chemical Industry Press.

Liu, J., Zou, S., Wu, J., Kobayashi, H., Zhao, H., & Fan, J. (2018). Green catalytic oxidation of benzyl alcohol over Pt/ZnO in base-free aqueous medium at room temperature. *Chinese Journal of Catalysis*, *39*(6), 1081-1089.

Liu, Y., & Zhang, R. (2020). Study of doped mesoporous ceria with tailored oxygen vacancies for enhances activity for ethylbenzene oxidation application. *Colloids and Surfaces A: Physicochemical and Engineering Aspects*, *603*, Article ID 125163.

Liu, Z.-G., Ji, L.-T., Liu, J., Fu, L.-L., & Zhao, S.-F. (2014). Influence of heat treatment on catalytic performance of Co–N–C/SiO2 for selective oxidation of ethylbenzene. *Journal of Molecular Catalysis A: Chemical*, *395*, 315-321.

Lu, C., Fu, Z., Liu, Y., Liu, F., Wu, Y., Qin, J., . . . Yin, D. (2010). A moderate and efficient method for oxidation of ethylbenzene with hydrogen peroxide catalyzed by 8-quinolinolato manganese(III) complexes. *Journal of Molecular Catalysis A: Chemical*, *331*(1-2), 106-111.

Lucky, S. S., Soo, K. C., & Zhang, Y. (2015). Nanoparticles in Photodynamic Therapy. *Chemical Reviews*, *115*(4), 1990-2042.

Ma, J., Liu, Y., Gao, P. F., Zou, H. Y., & Huang, C. Z. (2016). Precision improvement in dark-field microscopy imaging by using gold nanoparticles as an internal reference: a combined theoretical and experimental study. *Nanoscale*, *8*(16), 8729-8736.

Makhlouf, A. S. H. (2011). Current and advanced coating technologies for industrial applications. In A. S. H. Makhlouf & I. Tiginyanu (Eds.), *Nanocoatings and Ultra-Thin Films: Technologies and Application.* (pp. 3-23). Cambridge, UK: Woodhead Publishing.

Mallat, T., & Baiker, A. (2004). Oxidation of Alcohols with Molecular Oxygen on Solid Catalysts. *Chemical Reviews*, *104*(6), 3037-3058.

Marinoiu, A., Raceanu, M., Andrulevicius, M., Tamuleviciene, A., Tamulevicius, T., Nica, S., . . . Varlam, M. (2020). Low-cost preparation method of well dispersed gold nanoparticles on reduced graphene oxide and electrocatalytic stability in PEM fuel cell. *Arabian Journal of Chemistry*, *13*(1), 3585-3600.

Martynyuk, O., Kotolevich, Y., Pestryakov, A., Mota-Morales, J. D., & Bogdanchikova, N. (2015). Nanostructures constituted by unusually small silica nanoparticles modified with metal oxides as support for ultra-small gold nanoparticles. *Colloids and Surfaces A: Physicochemical and Engineering Aspects*, *487*, 9-16.

Masatake, H. (2003). When Gold Is Not Noble: Catalysis by Nanoparticles. *The Chemical Record*, *3*(2), 75-87.

Matsuyama, K., Tsubaki, T., Kato, T., Okuyama, T., & Muto, H. (2020). Preparation of catalytically active Au nanoparticles by sputter deposition and their encapsulation in metal-organic framework of Cu3(BTC)2. *Materials Letters*, *261*, Article ID 127124.

McClure, S. M., & Goodman, D. W. (2009). New insights into catalytic CO oxidation on Pt-group metals at elevated pressures. *Chemical Physics Letters*, *469*, 1-13.

Méndez-Cruz, M., Ramírez-Solís, J., & Zanella, R. (2011). CO oxidation on gold nanoparticles supported over titanium oxide nanotubes. *Catalysis Today, 166*(1), 172-179

Miah, A. T., Bharadwaj, S. K., & Saikia, P. (2017). Surfactant free synthesis of gold nanoparticles within meso-channels of non-functionalized SBA-15 for its promising catalytic activity. *Powder Technology*, *315*, 147-156.

Mo, L.-Q., Huang, X.-F., Wang, G.-C., Huang, G., & Liu, P. (2020). Full use of factors promoting catalytic performance of chitosan supported manganese porphyrin. *Scientific Reports*, *10*(1), Article ID 14132.

Moreau, F., Bond, G. C., & Taylor, A. O. (2005). Gold on titania catalysts for the oxidation of carbon monoxide: control of pH during preparation with various gold contents. *Journal of Catalysis*, *231*(1), 105-114.

Nadagouda, M. N., Speth, T. F., & Varma, R. S. (2011). Microwave-Assisted Green Synthesis of Silver Nanostructures. *Accounts of Chemical Research*, *44*(7), 469-478.

Narkhede, N., Patel, A., & Singh, S. (2014). Mono lacunary phosphomolybdate supported on MCM-41: synthesis, characterization and solvent free aerobic oxidation of alkenes and alcohols. *Dalton Trans*, *43*(6), 2512-2520.

Ndolomingo, M. J., & Meijboom, R. (2017). Selective liquid phase oxidation of benzyl alcohol to benzaldehyde by tert-butyl hydroperoxide over γ-Al2O3 supported copper and gold nanoparticles. *Applied Surface Science*, *398*, 19-32.

O'Keefe, M. A., Buseck, P. R., & Iijima, S. (1978). Computed crystal structure images for high resolution electron microscopy. *Nature*, *274*(5669), 322-324.

Oh, H. S., Yang, J. H., Costello, C. K., Wang, Y. M., Bare, S. R., Kung, H. H., & Kung, M. C. (2002). Selective Catalytic Oxidation of CO: Effect of Chloride on Supported Au Catalysts. *Journal of Catalysis*, *210*(2), 375-386.

Oliveira, A. P. S., Gomes, I. S., Neto, A. S. B., Oliveira, A. C., Filho, J. M., Saraiva, G. D., . . . Tehuacanero-Cuapa, S. (2017). Catalytic performance of MnFeSi composite in selective oxidation of styrene, ethylbenzene and benzyl alcohol. *Molecular Catalysis*, *436*, 29-42.

Pacioni, N., Borsarelli, C., Rey, V., & Veglia, A. (2015). Synthetic Routes for the Preparation of Silver Nanoparticles: A Mechanistic Perspective. In: Alarcon E., Griffith M., Udekwu K. (Eds) Silver Nanoparticle Applications. Engineering Materials (pp. 13-46), Copenhagen, Denmark: Springer Cham.

Peng, M., Ganesh, M., Rajangam, V., Palanichamy, M., & Jang, H. (2014). Solvent free oxidation of ethylbenzene over Ce-BTC MOF. *Arabian Journal of Chemistry*, *12*(7), 1358-1364.

Perego, C., & Villa, P. (1997). Catalyst preparation methods. *Catalysis Today*, *34*(3-4), 281-305.

Perumal, V., Hashim, U., Gopinath, S. C., Haarindraprasad, R., Poopalan, P., Liu, W. W., . . . Ruslinda, A. R. (2016). A new nano-worm structure from gold-nanoparticle mediated random curving of zinc oxide nanorods. *Biosens Bioelectron*, *78*, 14-22.

Pflästerer, D., & Hashmi, A. S. K. (2016). Gold catalysis in total synthesis–recent achievements. *Chemical Society Reviews*, *45*(5), 1331-1367.

Philip, A., Lihavainen, J., Keinänen, M., & Pakkanen, T. T. (2017). Gold nanoparticle-decorated halloysite nanotubes – Selective catalysts for benzyl alcohol oxidation. *Applied Clay Science*, *143*, 80-88.

Priecel, P., Salami, H. A., Padilla, R. H., Zhong, Z., & Lopez-Sanchez, J. A. (2016). Anisotropic gold nanoparticles: Preparation and applications in catalysis. *Chinese Journal of Catalysis*, *37*(10), 1619-1650.

Qiao, B., Liang, J.-X., Wang, A., Liu, J., & Zhang, T. (2016). Single atom gold catalysts for low-temperature CO oxidation. *Chinese Journal of Catalysis*, *37*(10), 1580-1586.

Rafiqul, I., Weber, C., Lehmann, B., & Voss, A. (2005). Energy efficiency improvements in ammonia production-perspectives and uncertainties. *Energy*, *30*(13), 2487-2504.

Raliya, R., Saha, D., Chadha, T. S., Raman, B., & Biswas, P. (2017). Non-invasive aerosol delivery and transport of gold nanoparticles to the brain. *Scientific Reports*, *7*(1), Article ID 44718.

Razzaq, H., Qureshi, R., Cabo-Fernandez, L., & Schiffrin, D. J. (2018). Synthesis of Au clusters-redox centre hybrids by diazonium chemistry employing double layer charged gold nanoparticles. *Journal of Electroanalytical Chemistry*, *819*, 9-15.

Rezaei, B., Boroujeni, M. K., & Ensafi, A. A. (2014). A novel electrochemical nanocomposite imprinted sensor for the determination of lorazepam based on modified polypyrrole@sol-gel@gold nanoparticles/pencil graphite electrode. *Electrochimica Acta*, *123*, 332-339.

Riaz, S., Bashir, M., Raza, M. A., Mahmood, A., & Naseem, S. (2015). Effect of Calcination on Structural and Magnetic Properties of Co-Doped ZnO Nanostructures. *IEEE Transactions on Magnetics*, *51*(11), 1-4.

Roduner, E. (2006). Size matters: why nanomaterials are different. *Chemical Society Reviews*, *35*(7), 583-592.

Rouquerol, J., Llewellyn, P., Navarrete, R., Rouquerol, F., & Denoyel, R. (2002). Assessing microporosity by immersion microcalorimetry into liquid nitrogen or liquid argon. In F. Rodriguez-Reinoso, B. McEnaney, J. Rouquerol, & K. Unger (Eds.), *Studies in Surface Science and Catalysis* (Vol. 144, pp. 171-176). Amsterdam, Netherlands: Elsevier.

Rouquerol, J., Llewellyn, P., & Rouquerol, F. (2007). Is the bet equation applicable to microporous adsorbents? In P. L. Llewellyn, F. Rodriquez-Reinoso, J. Rouqerol, & N. Seaton (Eds.), *Studies in Surface Science and Catalysis* (Vol. 160, pp. 49-56). Amsterdam, Netherlands: Elsevier.

Sandoval, A., Louis, C., & Zanella, R. (2013). Improved activity and stability in CO oxidation of bimetallic Au–Cu/TiO2 catalysts prepared by deposition–precipitation with urea. *Applied Catalysis B: Environmental*, *140-141*, 363-377.

Sankar, M., Nowicka, E., Carter, E., Murphy, D. M., Knight, D. W., Bethell, D., & Hutchings, G. J. (2014). The benzaldehyde oxidation paradox explained by the interception of peroxy radical by benzyl alcohol. *Nature Communications*, *5*(1), Article ID 3332.

Sharma, A. S., Kaur, H., & Shah, D. (2016). Selective oxidation of alcohols by supported gold nanoparticles: recent advances. *RSC Adv.*, *6*(34), 28688-28727.

Sheldon, R. A., Arends, I., & Hanefeld, U. (2007). *Green Chemistry and Catalysis*. New York, USA: John Wiley & Sons.

Shi, S., Chen, C., Wang, M., Ma, J., Gao, J., & Xu, J. (2014). Mesoporous strong base supported cobalt oxide as a catalyst for the oxidation of ethylbenzene. *Catalysis Science & Technology*, *4*(10), 3606-3610.

Simakin, A. V., Voronov, V. V., Kirichenko, N. A., & Shafeev, G. A. (2004). Nanoparticles produced by laser ablation of solids in liquid environment. *Applied Physics A*, *79*(4), 1127-1132.

Sperling, M. (2005). Chromium. In P. Worsfold, A. Townshend, & C. Poole (Eds.), *Encyclopedia of Analytical Science (Second Edition)* (pp. 113-126). Amsterdam, Netherlands: Elsevier.

Stacey, P., Kauffer, E., Moulut, J.-C., Dion, C., Beauparlant, M., Fernandez, P., . . . Wake, D. (2009). An International Comparison of the Crystallinity of Calibration Materials for the Analysis of Respirable -Quartz Using X-Ray Diffraction and a Comparison with Results from the Infrared KBr Disc Method. *The Annals of Occupational Hygiene, 53*(6), 639-649.

Stauffer, E., Dolan, J. A., & Newman, R. (2008). Chapter 8 - Gas Chromatography and Gas Chromatography-Mass Spectrometry. In E. Stauffer, J. A. Dolan, & R. Newman (Eds.), *Fire Debris Analysis* (pp. 235-293). Cambridge, MA: Academic Press.

Su, F.-Z., Ni, J., Sun, H., Cao, Y., He, H.-Y., & Fan, K.-N. (2008). Gold Supported on Nanocrystalline β-Ga2O3 as a Versatile Bifunctional Catalyst for Facile Oxidative Transformation of Alcohols, Aldehydes, and Acetals into Esters. *Chemistry – A European Journal*, *14*(24), 7131-7135.

Sun, D., & Sue, H.-J. (2015). Chapter 29 - Multifunctional polymer/ZnO nanocomposites: controlled dispersion and physical properties. In K. Friedrich & U. Breuer (Eds.), *Multifunctionality of Polymer Composites* (pp. 858-874). Norwich, NY: William Andrew Publishing.

Swihart, M. T. (2003). Vapor-phase synthesis of nanoparticles. *Current Opinion in Colloid & Interface Science*, *8*(1), 127-133.

Takale, B. S., Bao, M., & Yamamoto, Y. (2014). Gold nanoparticle (AuNPs) and gold nanopore (AuNPore) catalysts in organic synthesis. *Org Biomol Chem*, *12*(13), 2005-2027.

Takei, T., Akita, T., Nakamura, I., Fujitani, T., Okumura, M., Okazaki, K., . . . Haruta, M. (2012). Chapter 1 - Heterogeneous Catalysis by Gold. In B. C. Gates & F. C. Jentoft (Eds.), *Advances in Catalysis* (Vol. 55, pp. 1-126). Cambridge, MA: Academic Press.

Tan, K. H., Lee, H. W., Chen, J.-W., Dee, C. F., Majlis, B. Y., Soh, A. K., . . . Chang, W. S. (2017). Self-Assembled Heteroepitaxial AuNPs/SrTiO3: Influence of AuNPs Size on SrTiO3 Band Gap Tuning for Visible Light-Driven Photocatalyst. *The Journal of Physical Chemistry C*, *121*(25), 13487-13495.

Tang, Y., Xu, J., Wang, F., Zheng, Y., & Zhang, Z. (2020). Mechanism study on the oxidation of ethylbenzene: A theoretical and computational approach. *Computational and Theoretical Chemistry*, *1188*, Article ID 112974.

Titinchi, S. J. J., Von Willingh, G., Abbo, H. S., & Prasad, R. (2015). Tri- and tetradentate copper complexes: a comparative study on homogeneous and heterogeneous catalysis over oxidation reactions. *Catalysis Science Technology*, *5*(1), 325-338.

Titus, D., James Jebaseelan Samuel, E., & Roopan, S. M. (2019). Chapter 12 - Nanoparticle characterization techniques. In A. K. Shukla & S. Iravani (Eds.), *Green Synthesis, Characterization and Applications of Nanoparticles* (pp. 303-319). Amsterdam, Netherlands: Elsevier.

Torres, C. C., Alderete, J. B., Pecchi, G., Campos, C. H., Reyes, P., Pawelec, B., . . . Eimer, G. A. (2016). Heterogeneous hydrogenation of nitroaromatic compounds on gold catalysts: Influence of titanium substitution in MCM-41 mesoporous supports. *Applied Catalysis A: General*, *517*, 110-119.

Tsubota, S., Cunningham, D., Bando, Y., & Haruta, M. (1995). Preparation of nanometer gold strongly interacted with TiO 2 and the structure sensitivity in low-temperature oxidation of CO. *Studies in Surface Science and Catalysis*, *91*, 227-235.

Tsunoyama, H., Ichikuni, N., Sakurai, H., & Tsukuda, T. (2009). Effect of Electronic Structures of Au Clusters Stabilized by Poly(N-vinyl-2-pyrrolidone) on Aerobic Oxidation Catalysis. *Journal of the American Chemical Society*, *131*(20), 7086-7093.

Unnarkat, A. P., Singh, S., & Kalan, S. (2021). Ethylbenzene oxidation using cobalt oxide supported over SBA-15 and KIT-6. *Materials Today: Proceedings*, *45*, 3991-3996.

Vetrivel, S., & Pandurangan, A. (2004). Side-chain oxidation of ethylbenzene with tert-butylhydroperoxide over mesoporous Mn-MCM-41 molecular sieves. *Journal of Molecular Catalysis A: Chemical*, *217*(1), 165-174.

Villa, A., Wang, D., Su, D. S., & Prati, L. (2015). New challenges in gold catalysis: bimetallic systems. *Catalysis Science Technology*, *5*(1), 55-68.

Viswanathan, B., Sivasanker, S., & Ramaswamy, A. V. (2002). *Catalysis: Principles and Applications*. New Delhi, India: Narosa Publishing House.

Vourros, A., Garagounis, I., Kyriakou, V., Carabineiro, S. A. C., Maldonado-Hódar, F. J., Marnellos, G. E., & Konsolakis, M. (2017). Carbon dioxide hydrogenation over supported Au nanoparticles: Effect of the support. *Journal of CO2 Utilization*, *19*, 247-256.

Wang, D., Hao, Z., Cheng, D., & Shi, X. (2006). Influence of the calcination temperature on the Au/FeOx/Al2O3 catalyst. *Journal of Chemical Technology and Biotechnology*, *81*(7), 1246-1251.

Wang, H., Fan, W., He, Y., Wang, J., Kondo, J. N., & Tatsumi, T. (2013). Selective oxidation of alcohols to aldehydes/ketones over copper oxide-supported gold catalysts. *Journal of Catalysis*, *299*, 10-19.

Wei, H., Li, J., Yu, J., Zheng, J., Su, H., & Wang, X. (2015). Gold nanoparticles supported on metal oxides as catalysts for the direct oxidative esterification of alcohols under mild conditions. *Inorganica Chimica Acta*, *427*, 33-40.

Wolf, A., & Schüth, F. (2002). A systematic study of the synthesis conditions for the preparation of highly active gold catalysts. *Applied Catalysis A: General*, *226*(1), 1-13.

Wong, A. C., Wright, D. W., & Conrad, J. A. (2014). Functionalized Gold Nanoparticles for Detection of Cancer Biomarkers. In V. R. Preedy & V. B. Patel (Eds.), *General Methods in Biomarker Research and their Applications* (pp. 1-26). Dordrecht, Netherlands: Springer.

Wu, H., Pantaleo, G., Venezia, A., & Liotta, L. (2013). Mesoporous Silica Based Gold Catalysts: Novel Synthesis and Application in Catalytic Oxidation of CO and Volatile Organic Compounds (VOCs). *Catalysts*, *3*(4), 774-793.

Wu, H., Wang, L., Zhang, J., Shen, Z., & Zhao, J. (2011). Catalytic oxidation of benzene, toluene and p-xylene over colloidal gold supported on zinc oxide catalyst. *Catalysis Communications*, *12*(10), 859-865.

Xia, J. B., Cormier, K. W., & Chen, C. (2012). A Highly Selective Vanadium Catalyst for Benzylic C-H Oxidation. *Chemical Science*, *3*(7), 2240-2245.

Xu, S., Shi, G., Feng, Y., Chen, C., & Ji, L. (2020). Highly efficient transformation of ethylbenzene into acetophenone catalyzed by NHPI/Co(II) using molecular oxygen in hexafluoropropan-2-ol. *Molecular Catalysis*, *498*, Article ID 111244.

Yazid, H., Adnan, R., Hamid, S. A., & Farrukh, M. A. (2010). Synthesis and characterization of gold nanoparticles supported on zinc oxide via the deposition-precipitation method. *Turkish Journal of Chemistry*, *34*(4), 639-650.

Yesmurzayeva, N. N., Nurakhmetova, Z. A., Tatykhanova, G. S., Selenova, B. S., & Kudaibergenov, S. E. (2015). Catalytic Activity of Gold and Silver Nanoparticles Supported on Zinc Oxide. *Supramolecular Catalysis*, *2*, 1-8.

Yu, J., Li, J., Wei, H., Zheng, J., Su, H., & Wang, X. (2014). Hydrotalcite-supported gold catalysts for a selective aerobic oxidation of benzyl alcohol driven by visible light. *Journal of Molecular Catalysis A: Chemical*, *395*, 128-136.

Zanella, R., Delannoy, L., & Louis, C. (2005). Mechanism of deposition of gold precursors onto TiO2 during the preparation by cation adsorption and deposition–precipitation with NaOH and urea. *Applied Catalysis A: General*, *291*(1-2), 62-72.

Zanella, R., Giorgio, S., Henry, C. R., & Louis, C. (2002). Alternative methods for the preparation of gold nanoparticles supported on TiO2. *The Journal of Physical Chemistry B*, *106*(31), 7634-7642.

Zanella, R., & Louis, C. (2005). Influence of the conditions of thermal treatments and of storage on the size of the gold particles in Au/TiO2 samples. *Catalysis Today*, *107-108*(Supplement C), 768-777.

Zhan, B.-Z., & Thompson, A. (2004). Recent developments in the aerobic oxidation of alcohols. *Tetrahedron*, *60*(13), 2917-2935.

Zhang, G., Wang, D., Feng, P., Shi, S., Wang, C., Zheng, A., . . . Tian, Z. (2017). Synthesis of zeolite Beta containing ultra-small CoO particles for ethylbenzene oxidation. *Chinese Journal of Catalysis*, *38*(7), 1207-1215.

Zhao, X., Li, H., Zhang, J., Shi, L., & Zhang, D. (2016). Design and synthesis of NiCe@m-SiO2 yolk-shell framework catalysts with improved coke- and sintering-resistance in dry reforming of methane. *International Journal of Hydrogen Energy*, *41*(4), 2447-2456.

Zhao, Y., Xie, R., Lin, Y., Fan, G., & Li, F. (2018). Highly efficient solvent-free aerobic oxidation of ethylbenzene over hybrid Zn–Cr layered double hydroxide/carbon nanotubes nanocomposite. *Catalysis Communications*, *114*, 65-69.

Zheng, N., & Stucky, G. D. (2007). Promoting gold nanocatalysts in solvent-free selective aerobic oxidation of alcohols. *Chemical Communication, 37*, 3862-3864.

Zhu, J., Wang, P. C., & Lu, M. (2014). Selective oxidation of benzyl alcohol under solvent-free condition with gold nanoparticles encapsulated in metal-organic framework. *Applied Catalysis A: General*, *477*, 125-131.

Zhu, M., Wei, X., Li, B., & Yuan, Y. (2007). Copper-triethanolamine complex as efficient and active catalyst for selective oxidation of alkylarenes to phenyl ketones by tert-butylhydroperoxide. *Tetrahedron Letters*, *48*(52), 9108-9111.